ISTANBUL TECHNICAL UNIVERSITY ★ GRADUATE SCHOOL OF SCIENCE ENGINEERING AND TECHNOLOGY

MAXIMUM TORQUE PER AMPERE AND FLUX WEAKENING CONTROL OF IPM MOTORS FOR ELECTRICAL VEHICLES

M.Sc. THESIS

Ahmet Halit UNSAL

Department of Mechatronics Engineering

Mechatronics Engineering Programme

JANUARY 2016

ISTANBUL TECHNICAL UNIVERSITY ★ GRADUATE SCHOOL OF SCIENCE ENGINEERING AND TECHNOLOGY

MAXIMUM TORQUE PER AMPERE AND FLUX WEAKENING CONTROL OF IPM MOTORS FOR ELECTRICAL VEHICLES

M.Sc. THESIS

Ahmet Halit UNSAL
(518141002)

Department of Mechatronics Engineering

Mechatronics Engineering Programme

Thesis Advisor: Prof. Dr. Metin GOKASAN

20.01.2016

İSTANBUL TEKNİK ÜNİVERSİTESİ ★ FEN BİLİMLERİ ENSTİTÜSÜ

ELETRİKLİ ARACLAR İCİN KULLANILAN IPM MOTORLARIN AKIM BAŞINA MAKSİMUM TORK VE AKI ZAYIFLATMA YÖNTEMLERİYLE KONTROLÜ

YÜKSEK LİSANS TEZİ

Ahmet Halit ÜNSAL
(518141002)

Mekatronik Mühendisliği Anabilim Dalı

Mekatronik Mühendisliği Programı

Tez Danışmanı: Prof. Dr. Metin GÖKAŞAN

OCAK 2016

Ahmet Halit Ünsal, a **M.Sc.** student of ITU **Institute of Mechatronics Engineering** student ID **518141002**, successfully defended the **thesis** entitled "**MAXIMUM TORQUE PER AMPERE AND FLUX WEAKENING CONTROL OF IPM MOTORS FOR ELECTRICAL VEHICLES**", which he prepared after fulfilling the requirements specified in the associated legislations, before the jury whose signatures are below.

Thesis Advisor : **Prof. Dr. Metin GÖKAŞAN** ....
İstanbul Technical University

Jury Members : **Prof. Dr. Metin GÖKAŞAN** ....
İstanbul Technical University

Prof. Dr. Ata MUĞAN ....
İstanbul University

Asst. Prof. Dr. Özgür Turay KAYMAKÇI ....
Yıldız Technical University

Date of Submission : 25 November 2015
Date of Defense : 15 January 2016

To my spouse and children, I dedicate my dissertation work to my family and many friends. A special feeling of gratitude to my loving parents whose words of encouragement and push for tenacity ring in my ears. I also dedicate this dissertation to my many friends, I will always appreciate all they have done for me.

FOREWORD

I wish to thank my committee members who were more than generous with their expertise and precious time. A special thanks to Prof. Dr. Metin Gökaşan, my committee chairman and my advisor for his countless hours of reflecting, reading, encouraging, and most of all patience throughout the entire process. Thank you Prof. Dr. Ata Muağan, Asst. Prof. Dr. Özgür Turay for agreeing to serve on my committee. I would like to acknowledge and thank my school division for allowing me to conduct my research and providing any assistance requested. Special thanks goes to the members of staff development and human resources department for their continued support. Finally I would like to thank the beginning teachers, mentor-teachers and administrators in our school division that assisted me with this project. Their excitement and willingness to provide feedback made the completion of this research an enjoyable experience.

February 2016 Ahmet Halit ÜNSAL

TABLE OF CONTENTS

Page

FOREWORD ... **ix**
TABLE OF CONTENTS ... **xi**
ABBREVIATIONS ... **xiii**
LIST OF TABLES ... **xv**
LIST OF FIGURES ... **xvii**
SUMMARY ... **xix**
ÖZET ... **xxi**
1. THESIS INTRODUCTION ... **1**
1.1 Introduction ... 1
1.2 Motivation ... 1
1.3 Purpose of Thesis ... 2
1.4 Thesis Outline ... 3
2. REVIEW OF PREVIOUS WORK ... **5**
2.1 Literature Review ... 5
2.2 Troque Production ... 11
2.3 Previous Work On MTPA ... 14
2.3.1 A-priori methods ... 14
2.3.2 Control schemes based on biquadratic torque equation ... 15
2.3.3 Control schemes based on id, iq relationship ... 16
2.3.4 Control methods based on search algorithm ... 18
3. BURIED MAGNET MOTORS ... **21**
3.1 Introduction to IPMSM ... 21
3.2 Rotor Designs ... 21
3.3 Definition of Saliency ... 23
4. MATHEMATICAL ANALYSIS ... **25**
4.1 Introduction to Control Theory of IPMSM ... 25
4.2 Transformations ... 25
4.2.1 Clarke's transformation ... 25
4.2.2 Park's transformation ... 26
4.3 Motor Equations in the Rotor Reference Frame ... 27
4.4 The Permanent Magnet Synchronous Machine Equivalent Circuits and Mechanical Motor Model ... 29
5. CONTROL THEORY ... **31**
5.1 Introduction to Control Methods ... 31
5.2 Scalar Control ... 31
5.3 Vector Control ... 32
5.3.1 Field oriented control ... 32
5.3.2 Direct torque control ... 35
5.3.3 Maximum torque per ampere control algorithm ... 38
5.3.4 Flux-weakening control algorithms ... 42

5.3.5 Constant voltage constant power control 46
5.3.6 Constant-current-constant-power control 49
5.3.7 Voltage & current limited maximum torque control 51
6. SIMULATIONS 55
6.1 Drive System Simulations 55
6.2 Simulation Tools 55
6.3 IPMSM Drive Components 56
6.4 Design Procedure of the PI Controller 61
7. RESULTS 67
7.1 Simulation Results 67
7.1.1 Test 1: load = 100 Nm && speed = 3000 rpm 67
7.1.2 Test 2: load = 200 Nm && speed = 2000 rpm 72
7.1.3 Test 3: load = 200 Nm && speed = 5000 rpm 75
8. COMMENTS 81
8.1 Conclusion 81
8.2 Future Work 82
REFERENCES 83
CURRICULUM VITAE 89

ABBREVIATIONS

B	: Friction
PMSM	: Permanent magnet synchronous motor
IPMSM	: Internal permanent magnet synchronous motor
IPM	: Internal permanent magnet
PM	: Permanent magnet
CSI	: Current Source Inverter
VSI	: Voltage Source Inverter
D	: Direct axis
Q	: Quadrature axis
$\mathbf{f_c}$	: Crossover frequency
$\mathbf{i_a, i_b, i_c}$	: Three phase currents
$\mathbf{i_d}$	: D-axis current
$\mathbf{I_s}$	: Equivalent permanent magnet stator current
$\mathbf{i_q}$	: Q-axis current
$\mathbf{I_m}$	: Peak value of supply current
IGBT	: Insolate Gate Bipolar Transistor
IPM	: Interior Permanent Magnet
J	: Inertia
L	: Self inductance
$\mathbf{L_d}$	: D-axis self inductance
$\mathbf{L_{ls}}$	: Stator leakage inductance
$\mathbf{L_{dm}}$	: D-axis magnetizing inductance
$\mathbf{L_{qm}}$	: Q-axis magnetizing inductance
$\mathbf{L_q}$	: Q-axis self inductance
$\mathbf{L_s}$	: Equivalent self inductance per phase
p	: Number of poles
PI	: Proportional integral
$\mathbf{R_s}$	: Stator resistance
SPM	: Surface Permanent Magnet
BDCM	: Brushless DC Motor
$\mathbf{T_e}$	: Develop torque
$\mathbf{T_L}$	: Load torque
$\mathbf{V_a, V_b, V_c}$	: Three phase voltage
$\mathbf{V_d}$	: D-axis voltage
$\mathbf{V_q}$	: Q-axis voltage
$\boldsymbol{\rho}$	: Derivative operator
$\boldsymbol{\lambda_d}$	: Flux linkage due d axis
$\boldsymbol{\lambda_{pm}}$	: PM flux linkage or Field flux linkage
$\boldsymbol{\lambda_q}$	: Flux linkage due q axis
$\boldsymbol{\theta_r}$	: Rotor position
$\boldsymbol{\beta}$	: Current control angle
$\boldsymbol{\omega_m}$	: Rotor speed

ω_r	: Electrical speed
ω_{rated}	: Motor rated speed

LIST OF TABLES

Page

Table 3.1: Different conventions of naming of salient machines. 23

LIST OF FIGURES

Page

Figure 2.1: Variation in required i_q for different i_d values. Negative i_d produces more reluctance torque reducing the requirement for the i_q magnitude... 12
Figure 2.2: Magnetic torque produced by iq; the torque output is directly proportional to iq and only parameter dependence occurs if there is any change in permanent magnet flux. 12
Figure 2.3: Reluctance torque variation with id; positive id creates negative reluctance torque which eliminates any positive desired value for id..... 13
Figure 2.4: Phase current magnitudes for different id values; point of minimum phase current varies for different torque level. 13
Figure 2.5: id, iq lines for generating desired torques; intersections of the constant torque lines and MTPA line represent the optimum id, iq pairs for generating corresponding torques. 14
Figure 3.1: Different types of rotor configurations.. 22
Figure 4.1: Clarke and Park transform.. 26
Figure 4.2: Equivalent circuit for a salient machines direct axis............................ 30
Figure 4.3: Equivalent circuit for a salient machines quadrature axis..................... 30
Figure 5.1: Overview of available control strategies. 31
Figure 5.2: Phasor diagram of a PMSM in d-q frame.. 33
Figure 5.3: General control scheme of the Field Oriented Control. 34
Figure 5.4: DTC control layout.. 37
Figure 5.5: Torque angle... 38
Figure 5.6: Developed torque vs. torque angle of IPM motors............................... 39
Figure 5.7: The MTPA trajectory for IPM motors.. 42
Figure 5.8: Torque vs. speed characteristics of PMSM. 43
Figure 5.9: Power vs. speed characteristics of PMSM. 43
Figure 5.10: Current-limiting and voltage-limiting characteristics of PMSM.......... 45
Figure 5.11: Constant-voltage-constant power control of SPM motors. 49
Figure 5.12: The q-axis voltage trajectory of the CCCP control. 50
Figure 5.13: Constant-current-constant power control of SPM motors................... 51
Figure 5.14: Optimum current vector trajectory in the d, q frame for IPM motors.. 53
Figure 6.1: Vabc to Vdqo block.. 56
Figure 6.2: Idqo to Iabc block... 56
Figure 6.3: Simulink model of the IPMSM. 57
Figure 6.4: Torque Block.. 57
Figure 6.5: Speed Block.. 58
Figure 6.6: Voltage Source Inverter.. 58
Figure 6.7: PWM Current Controller.. 59
Figure 6.8: Control diagram for IPMSM. 60
Figure 6.9: Frequency response of the linearized system at ωn = 143.8 rad/sec. 65
Figure 6.10: Frequency response of the PI controller... 65

Figure 6.11: Frequency response of the combined system. 66
Figure 7.1: Test 1 ~ Speed analysis of the motor.. 68
Figure 7.2: Test 1 ~ Torque analysis of the motor. 68
Figure 7.3: Test 1 ~ D axis current (ref vs sim). 69
Figure 7.4: Test 1 ~ Q axis current (ref vs sim). 70
Figure 7.5: Test 1 ~ Stator current (ref vs sim). 70
Figure 7.6: Test 1 ~ Power analysis of the motor. 71
Figure 7.7: Test 1 ~ Power analysis of the battery. 71
Figure 7.8: Test 2 ~ Speed analysis of the motor.. 72
Figure 7.9: Test 2 ~ Torque analysis of the motor. 73
Figure 7.10: Test 2 ~ D axis current (ref vs sim). 74
Figure 7.11: Test 2 ~ Q axis current (ref vs sim). 74
Figure 7.12: Test 2 ~ Stator current (ref vs sim). 75
Figure 7.13: Test 3 ~ Speed analysis of the motor.. 76
Figure 7.14: Test 3 ~ Torque analysis of the motor. 76
Figure 7.15: Test 3 ~ D axis current (ref vs sim). 77
Figure 7.16: Test 3 ~ Q axis current (ref vs sim). 78
Figure 7.17: Test 3 ~ Stator current (ref vs sim). 78

MAXIMUM TORQUE PER AMPERE AND FLUX WEAKENING CONTROL OF IPM MOTORS FOR ELECTRICAL VEHICLES

SUMMARY

This thesis presents the basics of permanent magnet synchronous machine principles. A novel speed control algorithm for permanent magnet synchronous motors (PMSM) which maximizes efficiency without requiring phase current sensors is proposed in this thesis. The algorithm is described for a buried magnet type interior permanent magnet (IPM) motor but it is also suitable for surface mount type motors. The suggested algorithm implements maximum torque per ampere (MTPA) control in a PMSM drive system, considering the parameter variations due to magnetic saturation and change in temperature.

Interior permanent magnet synchronous motors (IPMSM) are commonly utilized for electric mobility since they have the ability to operate at a wide speed range while having a better torque density than other type of motors. Various control methods are discussed here and their abilities were compared to each other for different operation regions. In the constant torque operation region, MTPA (maximum torque per ampere) strategy is compared to the control strategy where the direct axis current set to zero. Above the base speed region, CCCP (constant current constant power) strategy was applied and when the rotor speed increased beyond the critical speed, control strategy is switched to MIP (maximum input power) control to sustain the optimal behavior of the machine. For each region, reference of the direct axis current is calculated in accordance with the generated reference of the stator current amplitude. Afterwards, quadrature axis current is calculated from the determined torque command and calculated direct axis current. In simulations, a vector control algorithm was utilized consisting of two main parts; outer control loop is being the speed and torque controller in cascaded form and the inner control loop is being the direct and quadrature axis current controller. The required information of the motor used in the simulations is obtained from the supplier while the DQ (direct-quadrature) axis inductances are measured for corresponding DQ axis currents. By doing so, simulation results became more realistic for both static and dynamic operations. This thesis presents the basics of permanent magnet synchronous machine principles and theoretical analysis supported with simulation results for variable speed operation regions.

In order to state the research objective of this thesis, a basic background is presented at the beginning. Then, the mathematical models of PMSMs are deduced, where the motor model in a d-q frame is a foundation of the vector control method. It is necessary to give a thorough analysis about the control principles of PMSMs for different operation conditions. Initially, the maximum torque per ampere (MTPA) control is described in detail in the constant torque region. Then, the FW control is explained in the constant power region. To simulate the control operations of PMSMs in different regions, a conventional motordrive system model is presented with its mechanical loads. Meanwhile, a closed-loop control, which implements MTPA control at low

speeds and FW control at high speeds, is implemented to operate the conventional inverter in the motor-drive system.

ELETRİKLİ ARACLAR İCİN KULLANILAN IPM MOTORLARIN AKIM BAŞINA MAKSİMUM TORK VE AKI ZAYIFLATMA YÖNTEMLERİYLE KONTROLÜ

ÖZET

Bu tez çalışmasında, elektrikli araçlar için kullanılabilecek sabit mıknatıslı senkron motorlar (PMSM) anlatılmıştır. Sabit mıknatıslı senkron motorların çalışması için gereken güç, uygun motor sürücüsü ve bataryalar aracılığıyla sağlanmıştır. Gerçekleştirilen kontrol metodu sayesinde bahsi geçen motorların maksimum tork yükleri altında elektrikli araç sistemleri için kullanımı mümkün hale getirilmiştir. Bu sistemler sayesinde daha fazla yük altında bu motorlar kullanılabilmektedir. Dolayısıyla aracın verimi artmaktadır. Kullanım alanı oldukça büyük olan ve gün geçtikçe büyüyen PMSM'li tahrik sistemleri, ilerde elektrikli araç sektöründe çalışacak öğrencilere bu bağlamda temel oluşturmada ve ışık tutmada muhakkak çok faydalı olacaktır.

Yapılan çalışmalar sonucunda sabit mıknatıslı motorların değişken çalışma bölgelerinde gerçekçi bir şekilde simülasyon ortamında analiz edilebileceği görülmüştür. Hareket analizinde belirlenen geri besleme bilgileri DSpace'in Microautobox ürünü aracılığıyla motor kontrolünde kullanılmıştır. Microautobox ile kontrol edilebilen sabit mıknatıslı motorların, istenilen hareket değerleriyle bütünleştiği görülmüştür.

Otomatik kontrol sistemleri kısaca bahsetmekte fayda vardır. Kontrol sistemleri günümüzde ileri toplumların günlük yaşantısına girmiş ve hemen hemen her alanda kullanılmaktadır. Evlerdeki otomatik çamaşır makineleri, otomatik bulaşık makineleri, termostatlı fırınlar veya diğer bir ifadeyle akıllı fırınlar, ütüler, endüstriyel ve araştırma alanında kullanılan robotlar, mikro işlemciler, bilgisayarlar, uzay taşıtları v.b. kontrol sistemleri, üretim ve yönetim kalitesini sürekli olarak arttırmakta olup, yaşam biçimimize olumlu bir şekilde etki etmektedirler. Kontrol sistemleri herhangi bir endüstri toplumunun tamamlayıcı bir parçası olup artan dünya nüfusunun ihtiyacı olan malzemeleri üretmek için gereklidirler. Kontrol sistemleri kısaca; enerji, malzeme veya diğer kaynakların akışını düzenleyen cihazlar olarak da tanımlanır. Bu cihazların düzenlenmesi; karmaşıklıklarına, görünüşlerine, kullanım amaçlarına ve işlevlerine göre değişir. Kontrol sistemleri, kontrol edilen büyüklüklerin değerlerini sabit tutarlar veya bu değerlerin, önceden belirlenmiş biçimde değişmesini sağlarlar.

Bilim ve teknoloji ilerledikçe insan kas gücünün üretimdeki payı azalmaktadır. Üretim, makine ile yapılan veya insan gücüyle yapılan üretim diye ayrılsa, makine tarafı sürekli olarak artma eğilimindedir. Makinelerin kullanımı da yine insan denetimi yerine başka makineler veya teçhizatlar yardımıyla yapılmaya çalışılmaktadır. Makinelerle yapılan üretimde, neredeyse çalışan sistem üzerinde insan denetimi yok denecek düzeydedir. Otomatik kontrol sistemleri, çalışan sistemlerin insan gücüne gerek kalmadan kontrol edilmesini konu olarak ele alır. Dünyada emek yoğun üretim,

pahalı bir üretim yöntemi haline gelmiştir. Otomasyon sistemi ile üretim, daha ekonomik olmaktadır. Otomasyon, üretimin her aşamasına hızlı bir şekilde girmeye devam etmektedir. Böylece daha ucuz ve standardı önceden belirlenen ölçülerde üretim yapılabilmektedir.

Endüstriyel kontrol alanındaki teknolojik gelişmeler ve yukarıda da bahsedildiği gibi otomatik kontrolün ve otomasyonun hızla artan konumu, birçok özel motorun ortadan kalkmasına, uygulamaların çoğunun nispeten az sayıda motor tipiyle gerçekleşmesine, dikkatin servo motorlara, kaynak ve kontrol düzenlemelerine kaymasına neden olmuştur. Böylece üstün bir performans ve esneklik sağlanmıştır. Sabit hızlı bir motordan daha fazlasının gerekli olduğu pozisyonlama, yüksek kararlılık, periyodik çalışma, dinamik yük ve hız değişikliği gibi durumlarda servo sistem vazgeçilmez tercih olmaktadır. Bu bağlamda tezde hali hazırda büyük ilerlemeler kaydeden elektrikli araçlara yönelik motor kontrolleri hakkında bilgiler verilmektedir.

Sabit mıknatıslı senkron motorlar (PMSM), sahip oldukları avantajları dolayısıyla günümüzde daha çok tercih edilir duruma gelmiştir. Avantajlarının başlıcaları; yüksek verim, güvenilir çalışma ortamı, daha az bakım, sessiz çalışma, kolay soğutma, uzun ömür ve kolay kontrol edilebilme şeklinde belirtilebilir. Bununla beraber; karmaşık bir kontrol yapısına sahip olmaları, pahalı bir sistem oluşu, rotor pozisyonunun algılanabilmesi için pozisyon sensörlerine ihtiyaç duyması gibi dezavantajlara da sahiptir. Pozisyon sensörlerinin kullanılmadığı durumlarda ilave algoritmalar gerekir. Ancak günümüzde gelinen noktada geliştirilen yöntemlerle, bu motorların dezavantajları önemsiz duruma gelmeye başlamış ve kullanımları artmıştır. Otomotiv sektörü, uzay ve bilgisayar teknolojileri, tıp elektroniği, askeri alanlar, robotik uygulamalar ve ev ürünlerinde sıkça kullanılmakta ve kullanım alanları gittikçe genişlemektedir. Bir PMSM motor, üç faz sargılı stator, sabit mıknatıslı rotor, geri besleme üniteleri, evirici ve sürücü katmanı ile denetleyici yapılarından oluşmaktadır. Stator sargılarının enerjilendirilmesi rotor pozisyonuna göre yapılır. Rotor konumu algılayıcılar ile belirlenir. Bunun dışında, sürücü için akım veya gerilim bilgileri de ölçülerek kullanılmalıdır. Hız ve konum denetimi için en çok Hall ya da optik sensörler kullanılır. Rotor pozisyonunun sensörsüz olarak belirlendiği teknikler de giderek yaygınlaşmaktadır.

PMSM motorlarda motorun akımı, torku, rotor konumu ve hızı gibi parametreler çeşitli kontrol yöntemleri kullanılarak kontrol edilir. Bu kontrol şu şekilde olmaktadır; denetleyicinin ürettiği kontrol sinyali, seçilen kontrol algoritmasına göre PWM sinyallerinin durumunu kontrol eder. Bu şekilde denetleyici tarafından motor parametreleri kontrol edilir ki, denetleyici hem yazılım, hem de donanım yapılarından oluşur.

PMSM motorların kontrolünde yapılarının basitliği nedeniyle ve birçok uygulamalarda yeterli verimi karşılaması nedeniyle klasik denetleyiciler (PI ve PD tipi) kullanılır. Ancak denetlenecek sistemin modeline ihtiyaç duymaları ve en uygun kazanç değerlerinin deneme yanılmayla belirlenmesi dezavantaj oluşturmakta; sinüzoidal ve ani değişimlerdeki performansları yetersiz olmaktadır. Dolayısıyla, PI ve PD tipi denetleyiciler hassasiyet aranmayan uygulamalarda sıkça kullanılmaktadır. Çok hassas denetim gerektiren uygulamalarda ise modern denetim teknikleri tercih edilmektedir. Günümüzde modern denetim tekniklerine, bulanık mantık, yapay sinir ağları, genetik algoritma, sinirsel bulanık denetleyiciler örnek verilebilir.

Daha öncede bahsedildiği üzere, bu tez sabit mıknatıslı senkron makine ilkelerinin temellerini göstermektedir. Sabit mıknatıslı senkron motorlar (PMSM) için motor verimliliğini maksimize edicek yeni bir hız kontrol algoritması bu tezde önerilmiştir. Algoritma, gömülü mıknatıs tipi (IPM) motorlar için uygulanmıştır. Ancak yüzey tipi motorlar için de uygundur. Önerilen algoritma sayesinde manyetik doygunluk ve sıcaklık değişimleri göz önünde bulundurarak, maksimum tork amper (MTPA) kontrolünü uygular.

Gömülü sabit mıknatıslı motorlar iyi bir tork yoğunluğuna sahip oldukları için yaygın olarak elektrikli araçlarda kullanılmaktadır. Çeşitli kontrol yöntemleri burada tartışılmıştır, ve farklı çalışma bölgeleri için karşılaştırılmıştır. Sabit tork operasyon bölgesinde, MTPA (maksimum tork amper) kontrol stratejisi ve D ekseni akımını sıfıra çeken kontrol metodu karşılaştırıldığında, motordan elde edilebilecek maksimum torkun MTPA metodu ile en verimli şekilde elde edildiği gözlemlenmiştir. Bunun yanı sıra D ekseni akımını sıfıra çekerek, diğer metotda elde edilen torklara çıkılamamıştır. Motor kontrolü baz hızının üstündeki bölgelerde "sabit akım sabit güç" (CCCP) kontrol stratejisi uygulanarak çalıştırılmış, ve rotor hızının kritik hız ve ötesinde arttığı koşullarda, kontrol stratejisi makinenin optimum davranışını sürdürmek için "maksimum giriş gücü" (MIP) algoritmasına uygun olarak değiştirilmiştir. Her bölgede, doğru eksen akımı (id) için referans, stator akımı belirlenerek oluşturulmuş ve buna bağlı olarak da çeyrek eksen akımı (iq) hesaplanmıştır. Simulasyonlar için, iki ana bölümden oluşan bir vektör kontrol algoritması kullanılmıştır. Dış denetim döngüsü ardışık biçimde oluşturulmuş ve bu sayede hız ve tork kontrol edilmiştir. İç kontrol döngüsünde ise akım kontrol edilmiştir. DQ eksen endüktansları, DQ eksen akımlarına karşılık gelecek şekilde sürekli biçimde değiştirilmiştir. Simülasyonlarda kullanılan motorun gerekli bilgileri tedarikçiden elde edilmiştir. Bu şekilde, simülasyon sonuçları hem statik hem de dinamik işlemler için daha gerçekçi hale getirilmiştir.

Bu tezin araştırma amacını belirtmek için, kullanılan motor çeşidi hakkında temel arka plan bilgileri tezin başında yer almaktadır. PMSM'nin matematiksel modeller açıklanarak, oluşan DQ eksen akımları anlatılmıştır. Farklı çalışma koşulları için değişik kontrol prensipleri hakkında kapsamlı bir analiz verilmiştir. Farklı operasyon bölgelerinde PMSM kontrol işlemlerini simüle etmek için, geleneksel motor sürücü sistemi modeli mekanik yüklerele gösterilmiştir. Bu arada, yüksek hızlarda akı zayıflatma (FW) kontrol metodu kullanılmıştır. Kapalı çevrim kontrol uygulanarak, motor tahrik sistemi konvansiyonel motor sürücüsü ile tahrik edilmiştir.

1. THESIS INTRODUCTION

1.1 Introduction

Permanent Magnet Synchronous Motors (PMSM) have long been used in servo motor drives and has lately become more popular in lager motors for industrial applications. Another target application for PMSM is electric vehicles, were its small size and robustness is a big advantage compared to Induction or DC motors. This development of PMSM has been made possible according to the introduction of new magnetic materials like Neodymium Iron Boron (Nd2Fe14B) and Samarium Cobalt (SmCo5). These types of magnets have a high energy density and high resistance for de-magnetization. Previously Ferrite or Aluminum Nickel Cobalt (AlNiCo) magnet had to be used, this made the motors bulky and they were susceptible to demagnetization if the control of the motor current was incorrect. The demagnetization problem was one of the reasons that the $id = 0$ control strategy was adopted [2], this works well for round rotors but for a salient rotor a couple of their advantages are lost. It limits the motors speed range and the maximum efficiency cannot be reached. To take advantage of the properties of modern magnetic materials, a new approach to controlling the motors has got possible them has to be taken.

The current vector control algorithm of an IPMSM in different speed operation regions were explored. Form the theoretical analyses, the optimal behavior of the IPMSM can be achieved by considering two phase control algorithm: maximum torque per ampere (MTPA) control strategy in constant torque region, flux-weakening control strategy in high-speed region. The algorithm provides robust current regulation with maximum efficiency and torque capability for IPMSM. In different region, the optimum d-axis current command can be calculated according to different control strategy. The q-axis current command is determined from the torque command and d-axis current.

1.2 Motivation

Modeling and simulation is usually used in designing PM drives compared to building system prototypes because of the cost. Having selected all components, the simulation process can start to calculate steady state and dynamic performance and losses that would have been obtained if the drive were actually constructed. This practice reduces time, cost of building prototypes and ensures that requirements are achieved.

In works available until now ideal components have been assumed in the inverter feeding the motor and simulations have been carried out. The voltages and currents in different parts of the inverter have not been obtained and hence the losses and efficiency cannot be calculated. In this work, the simulation of a PM motor drive system is developed using Simulink. The simulation circuit includes all realistic components of the drive system. This enables the calculation of currents and voltages in different parts of the inverter and motor under transient and steady conditions. The losses in different parts are calculated. A comparative study associated with hysteresis and PWM control techniques in current controllers has been made. A speed controller has also been designed for closed loop operation of the drive. Design method for the PI controller is also given.

1.3 Purpose of Thesis

Though the presence of rotor saliency provides an additional source of torque in IPMs, utilizing that advantage adds complexity in the control of these machines. IPMs produce sinusoidal 3-phase back EMF voltages that provide constant power if 3-phase sinusoidal current is maintained in the stator. Phase current components in phase with corresponding back EMF voltages (Quadrature axis current), produce only magnetic torque but do not contribute in producing reluctance torque. The current components 90 degrees out of phase with back EMF voltages (Direct axis current), produce reluctance torque in conjunction with quadrature axis currents. Thus, there exist an infinite number of current vectors providing the same amount of torque. For most efficient operation, the current vector with the lowest possible magnitude should be chosen to reduce winding losses. Significant variation in motor parameters and operating conditions make it difficult to come up with optimum current vectors. In this thesis, a current minimizing control strategy, also known as Maximum Torque per Ampere (MTPA) control for IPMs is proposed. Rather than using conventional vector control, a method based on only DC link power measurement is suggested. Parameter variation arising from different sources is also considered in the control application.

1.4 Thesis Outline

Chapter 2 presents the literature review of control strategies developed over the years for permanent magnet synchronous motors. General theory of the permanent magnet motors is also discussed here, with focusing on different control algorithms. The chosen control strategy and previous work done on it is discussed.

Chapter 3 presents the review of general theory of permanent magnet synchronous motors, with focus on different rotor types and their properties, the chapter also present the motor used in this project.

Chapter 4 gives a presentation of mathematical equations that can be used for a PMSM.

Chapter 5 presents a more detailed investigation of the preferred control method, maximum torque per ampere. It will also present the difference in control strategies for different rotor types.

Chapter 6 presents the simulink model of the motor and the control algorithms.

Chapter 7 presents the individual simulations and their results of the models from chapter 6.

Chapter 8 discusses the result of the work and give suggestions for improvements and future work.

2. REVIEW OF PREVIOUS WORK

2.1 Literature Review

PM motor drives have been a topic of interest for the last twenty years. Different authors have carried out modeling and simulation of such drives.

In 1986 Sebastian, T., Slemon, G. R. and Rahman, M. A. [1] reviewed permanent magnet synchronous motor advancements and presented equivalent electric circuit models for such motors and compared computed parameters with measured parameters. Experimental results on laboratory motors were also given.

In 1986 Jahns, T.M., Kliman, G.B. and Neumann, T.W. [2] discussed that interior permanent magnet (IPM) synchronous motors possessed special features for adjustable speed operation which distinguished them from other classes of ac machines. They were robust high power density machines capable of operating at high motor and inverter efficiencies over wide speed ranges, including considerable range of constant power operation. The magnet cost was minimized by the low magnet weight requirements of the IPM design. The impact of the buried magnet configuration on the motor's electromagnetic characteristics was discussed. The rotor magnetic saliency preferentially increased the quadrature-axis inductance and introduced a reluctance torque term into the IPM motor's torque equation. The electrical excitation requirements for the IPM synchronous motor were also discussed. The control of the sinusoidal phase currents in magnitude and phase angle with respect to the rotor orientation provided a means for achieving smooth responsive torque control. A basic feed forward algorithm for executing this type of current vector torque control was discussed, including the implications of current regulator saturation at high speeds. The key results were illustrated using a combination of simulation and prototype IPM drive measurements.

In 1988 Pillay and Krishnan, R. [3], presented PM motor drives and classified them into two types such as permanent magnet synchronous motor drives (PMSM) and brushless dc motor (BDCM) drives. The PMSM has a sinusoidal back emf and requires sinusoidal stator currents to produce constant torque while the BDCM has a trapezoidal back emf and requires rectangular stator currents to produce constant torque. The PMSM is very similar to the wound rotor synchronous machine except that the PMSM that is used for servo applications tends not to have any damper windings and excitation is provided by a permanent magnet instead of a field winding. Hence the d, q model of the PMSM can be derived from the well known model of the synchronous machine with the equations of the damper windings and field current dynamics removed. Equations of the PMSM are derived in rotor reference frame and the equivalent circuit is presented without dampers. The damper windings are not considered because the motor is designed to operate in a drive system with field-oriented control. Because of the nonsinusoidal variation of the mutual inductances between the stator and rotor in the BDCM, it is also shown in this paper that no particular advantage exists in transforming the abc equations of the BCDM to the d, q frame.

As an extension of his previous work, Pillay, P. and Krishnan, R. in 1989 [4] presented the permanent magnet synchronous motor (PMSM) which was one of several types of permanent magnet ac motor drives available in the drives industry. The motor had a sinusoidal flux distribution. The application of vector control as well as complete modeling, simulation, and analysis of the drive system were given. State space models of the motor and speed controller and real time models of the inverter switches and vector controller were included. The machine model was derived for the PMSM from the wound rotor synchronous motor. All the equations were derived in rotor reference frame and the equivalent circuit was presented without dampers. The damper windings were not considered because the motor was designed to operate in a drive system with field-oriented control. Performance differences due to the use of pulse width modulation (PWM) and hysteresis current controllers were examined. Particular attention was paid to the motor torque pulsations and speed response and experimental verification of the drive performance were given.

Morimoto, S., Tong, Y., Takeda, Y. and Hirasa, T. in 1994 [5], in their paper aimed to improve efficiency in permanent magnet (PM) synchronous motor drives. The controllable electrical loss which consisted of the copper loss and the iron loss could be minimized by the optimal control of the armature current vector. The control algorithm of current vector minimizing the electrical loss was proposed and the optimal current vector could be decided according to the operating speed and the load conditions. The proposed control algorithm was applied to the experimental PM motor drive system, in which one digital signal processor was employed to execute the control algorithms, and several drive tests were carried out. The operating characteristics controlled by the loss minimization control algorithm were examined in detail by computer simulations and experimental results.

The paper in 1997 by Wijenayake, A.H. and Schmidt, P.B. [6], described the development of a two-axis circuit model for permanent magnet synchronous motor (PMSM) by taking machine magnetic parameter variations and core loss into account. The circuit model was applied to both surface mounted magnet and interior permanent magnet rotor configurations. A method for on-line parameter identification scheme based on no-load parameters and saturation level, to improve the model, was discussed in detail. Test schemes to measure the equivalent circuit parameters, and to calculate saturation constants which govern the parameter variations were also presented.

In 1997 Jang-Mok, K. and Seung-Ki, S. [7], proposed a novel flux-weakening scheme for an Interior Permanent Magnet Synchronous Motor (IPMSM). It was implemented based on the output of the synchronous PI current regulator reference voltage to PWM inverter. The on-set of flux weakening and the level of the flux were adjusted inherently by the outer voltage regulation loop to prevent the saturation of the current regulator. Attractive features of this flux weakening scheme included no dependency on the machine parameters, the guarantee of current regulation at any operating condition, and smooth and fast transition into and out of the flux weakening mode. Experimental results at various operating conditions including the case of detuned parameters were presented to verify the feasibility of the proposed control scheme.

Bose, B. K., in 2001 [8], presented different types of synchronous motors and compared them to induction motors. The modeling of PM motor was derived form the model of salient pole synchronous motor. All the equations were derived in synchronously rotating reference frame and was presented in the matrix form. The equivalent circuit was presented with damper windings and the permanent magnet was represented as a constant current source. Some discussions on vector control using voltage fed inverter were given.

Bowen, C., Jihua, Z. and Zhang, R. in 2001 [9], addressed the modeling and simulation of permanent magnet synchronous motor supplied from a six step continuous inverter based on state space method. The motor model was derived in the stationary reference frame and then in the rotor reference frame using Park transformation. The simulation results obtained showed that the method used for deciding initial conditions was very effective.

In 2002 Mademlis, C. and Margaris, N. [10], presented an efficiency optimization method for vector-controlled interior permanent-magnet synchronous motor drive. Based on theoretical analysis, a loss minimization condition that determines the optimal q-axis component of the armature current was derived. Selected experimental results were presented to validate the effectiveness of the proposed control method.

In 2004, Jian-Xin, X., Panda, S. K., Ya-Jun, P., Tong Heng, L. and Lam, B. H. [11] applied a modular control approach to a permanent-magnet synchronous motor (PMSM) speed control. Based on the functioning of the individual module, the modular approach enabled the powerfully intelligent and robust control modules to easily replace any existing module which did not perform well, meanwhile retaining other existing modules which were still effective. Property analysis was first conducted for the existing function modules in a conventional PMSM control system: proportional-integral (PI) speed control module, reference current-generating module, and PI current control module. Next, it was shown that the conventional PMSM controller was not able to reject the torque pulsation which was the main hurdle when PMSM was used as a high-performance servo. By virtue of the internal model, to nullify the torque pulsation it was imperative to incorporate an internal model in the feed-through path. This was achieved by replacing the reference current-generating module with an iterative learning control (ILC) module. The ILC module records the cyclic torque and reference current signals over one entire cycle, and then uses those signals to update the reference current for the next cycle. As a consequence, the torque pulsation could be reduced significantly. In order to estimate the torque ripples which might exceed certain bandwidth of a torque transducer, a novel torque estimation module using a gain-shaped sliding-mode observer was further developed to facilitate the implementation of torque learning control. The proposed control system was evaluated through real-time implementation and experimental results validated the effectiveness.

Araujo, R.E., Leite, A.V. and Freitas, D.S. in 1997 [12], mentioned the different simulation tools available and the benefits that were obtained by accelerating the process for the development of visual design concepts. Among various software packages for simulation of electronic circuits, like SPICE and SABER, EMTP, EUROSTAG, or for specialized simulations tools for power electronics system like SIMPLORER, POSTMAC, SIMSEN, ANSIM, and PSCAD, they had chosen MATLAB/Simulink. MATLAB/Simulink had user-friendly environment, visual design, Real-Time Workshop and libraries of models for the various components of a power electronic system.

Ong, C in 1998 [13], explained the need for powerful computation tools to solve complex models of motor drives. Among the different simulation tools available for dynamic simulation he had chosen MATLAB/SIMULINK® as the platform for his book because of the short learning curve required to start using it, its wide distribution, and its general purpose nature.

Macbahi, H. Ba-razzouk, A. Xu, J. Cheriti, A. and Rajagopalan, V. in 2000 [14], mentioned that a great number of universities and researchers used the MATLAB/SIMULINK software in the field of electrical machines because of its advantages such as user friendly environment, visual oriented programming concept, non-linear standard blocks and a large number of toolboxes for special applications.

In 1997 Reece, J.H., Bray, C.W., Van Tol, J.J. and Lim, P.K. [15], discussed three possible computer simulation tools such as PSpice, HARMFLO and the Electromagnetic Transients Program (EMTP) in their project on power systems containing adjustable speed drives. They selected EMTP as the primary simulation tool because of its broad range of capabilities, which were well matched to their problem.

French, C.D., Finch, J.W. and Acarnley, P.P. in 1998 [16], had found that in recent years the increase in desktop computing power has lead to an increase in the sophistication of both design and simulation tools available to the design engineer. One such tool becoming more wide spread amongst academia and industry was Mathwork’s Simulink / Matlab package. This paper described how Simulink could be used as an integrated development environment for simulation and real time control of electric motor drive systems. This was carried out with the aid of motor models together with simulation and real time control circuits. It was demonstrated how such a set-up could be used as a cost effective control system rapid prototyping scheme.

Onoda, S. and Emadi, A. in 2004 [17], had developed a modeling tool to study automotive systems using the power electronics simulator (PSIM) software. PSIM was originally made for simulating power electronic converters and motor drives. This user- friendly simulation package was able to simulate electric/electronic circuits.

Venkaterama, G. [18]; had developed a simulation for permanent magnet motors using Matlab/simulink. The motor was a 5 hp PM synchronous line start type. Its model included the damper windings required to start the motor and the mathematical model was derived in rotor reference frame. The simulation was presented with the plots of rotor currents, stator currents, speed and torque.

Simulink PM Synchronous Motor Drive demo circuit (2005) [19] used the AC6 block of SimPowerSystems library. It modeled a permanent magnet synchronous motor drive with a braking chopper. The PM synchronous motor was fed by a PWM voltage source inverter, which was built using a Universal Bridge Block. The speed control loop used a PI regulator to produce the flux and torque references for the vector control block. The vector control block computed the three reference motor line currents corresponding to the flux and torque references and then fed the motor with these currents using a three-phase current regulator. Motor current, speed, and torque signals were available at the output of the block.

The demo circuit (2005) in Simulink for Permanent magnet synchronous motor fed by PWM inverter [20] had a three-phase motor rated 1.1 kW, 220 V, 3000 rpm. The PWM inverter was built entirely with standard Simulink blocks. Its output went through Controlled Voltage Source blocks before being applied to the PMSM block's stator windings. Two control loops were used. The inner loop regulated the motor's stator currents. The outer loop controlled the motor's speed. Line to line voltages, three phase currents, speed and torque were available at the output of the scope blocks.

In the above works, none of them have considered a real drive system simulation in Simulink operating at constant torque and flux weakening regions.

2.2 Troque Production

The torque production in an IPM is a function of ϕ_M, i_d, i_q, L_d and L_q. There are an infinite number of iq and id combinations which can produce the same amount of torque. Introducing the inductance drop even complicates i_q and i_d selection further.

The torque produced by any IPM can be split into two components. The component arising from the permanent magnet flux is called reactance torque or magnetic torque and expressed by:

$$T_{magnetic} = \frac{3}{2}\frac{p}{2}\phi_M i_q \tag{2.1}$$

The other component arising from rotor saliency can be called reluctance torque and expressed by:

$$T_{reluctance} = \frac{3}{2}\frac{p}{2}(L_d - L_q) i_d i_q \tag{2.2}$$

Since permanent magnets have higher reluctance or lower permeability than iron, inductance along the d-axis is usually lower than that along the q-axis [26]. Thus, for conventional IPMs L_d is smaller than L_q. This in turns necessitates introduction of negative i_d in order to produce any positive torque.

Figure 2.1 shows the variation required in i_q for different i_d in producing a particular amount of torque. A constant parameter motor model was considered to avoid complexity. Negative id reduces the required amount of i_q by aiding in the reluctance torque generation. Figure 2.2 shows the amount of torque produced by ϕ_M and which is essentially directly proportional to the magnitude of i_q. Figure 2.3 shows the contribution of reluctance torque arising from i_d. Since a positive value of direct axis current is opposing the magnetic torque, a positive i_d is never desired. As shown in Figure 2.4, for any torque level, there exists a particular i_q, i_d pair that causes minimum phase currents. Since resistive loss in the stator solely depends on phase current magnitudes, it is always preferred to operate the motor as close as possible to these i_q, i_d pairs. Since it is similar to maximizing the torque output for a particular amount of current, the operation scheme is called Maximum Torque per Ampere (MTPA).

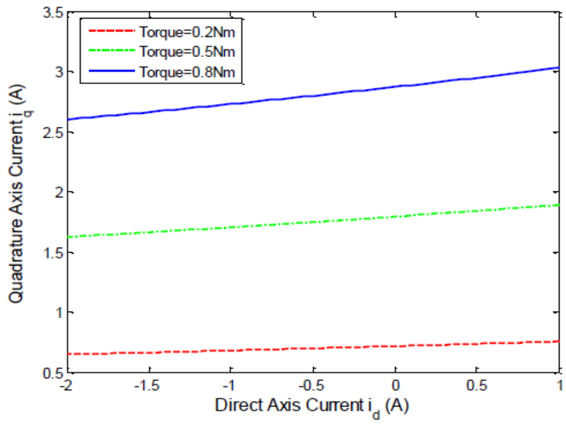

Figure 2.1: Variation in required i_q for different i_d values. Negative i_d produces more reluctance torque reducing the requirement for the i_q magnitude.

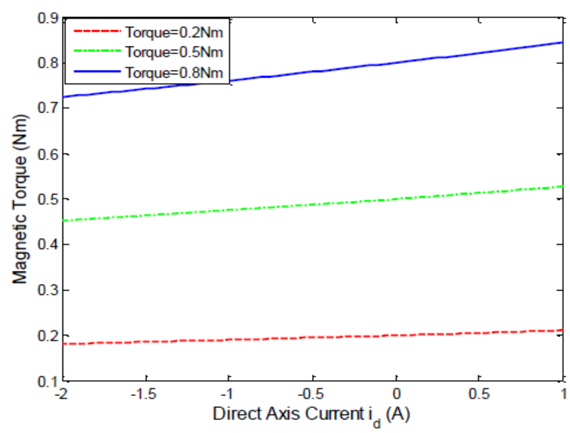

Figure 2.2: Magnetic torque produced by iq; the torque output is directly proportional to iq and only parameter dependence occurs if there is any change in permanent magnet flux.

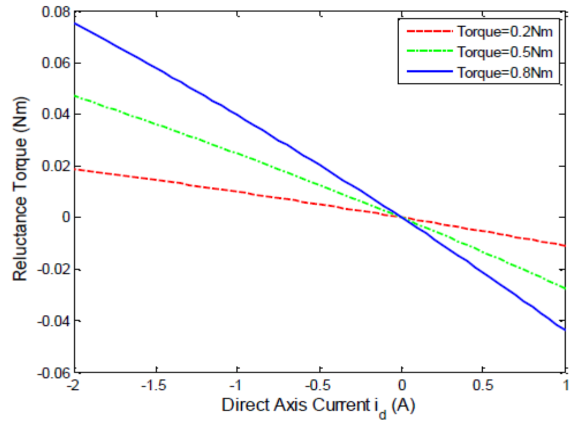

Figure 2.3: Reluctance torque variation with id; positive id creates negative reluctance torque which eliminates any positive desired value for id.

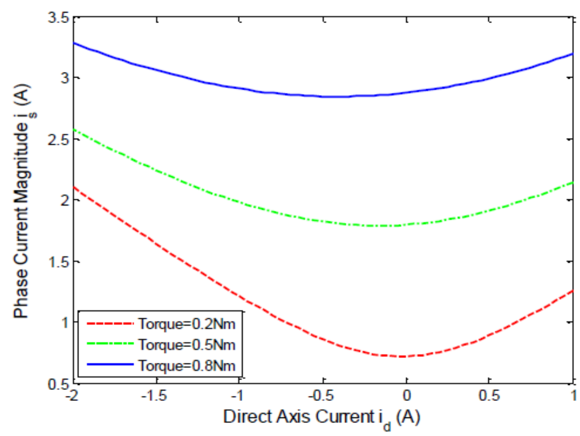

Figure 2.4: Phase current magnitudes for different id values; point of minimum phase current varies for different torque level.

The concept of MTPA can be better realized from closer observation of Figure 2.5. The MTPA line shows the i_q, i_d pairs which produce desired torque with the minimum possible current magnitudes. The concave curves show the constant torque lines indicating all the i_q, i_d pairs falling on those lines produce the same amount of torque. But as discussed earlier, there exists only one particular i_q, i_d pair that produces desired torque with minimum current magnitude. These desired pairs are the points where constant torque lines intersect with MTPA line. The dotted quarter circle represents the maximum allowed current limit for the particular motor.

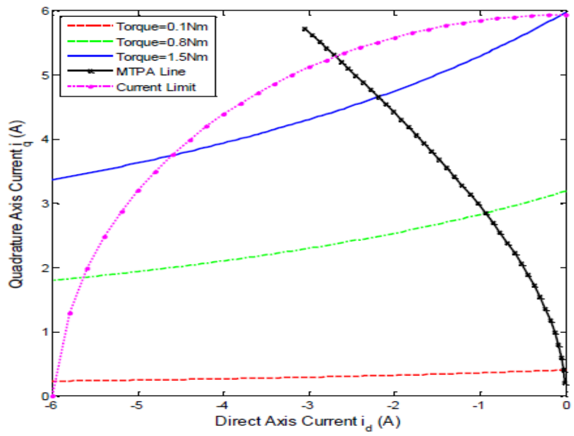

Figure 2.5: id, iq lines for generating desired torques; intersections of the constant torque lines and MTPA line represent the optimum id, iq pairs for generating corresponding torques.

2.3 Previous Work On MTPA

Developing a control strategy for MTPA operation has drawn considerable attention and various solutions have been proposed so far. Early researchers proposed techniques based on constant parameter motor models which fail to give satisfactory performance over the entire operating region. Later, control schemes considering magnetic saturation and temperature effects were proposed. With the advancement in processing power of DSP controllers, more computation intensive algorithms have been proposed in recent years. Based on their operational strategies, proposed control schemes can be roughly grouped into two main categories;

- A priori methods (based on premade tables, polynomials or solution of equations based on motor model and parameters),
- Methods based on a search algorithm.

2.3.1 A-Priori Methods

Most of the control strategies proposed so far use premade tables, estimation polynomials or utilize equations to compute MTPA operating points. Two major techniques implementing a-priori methods are observed in the literature as

- Control schemes based on the solution of the biquadratic equation(Methods that directly compute i_q, i_d at a given condition),

- Control schemes based on i_q, i_d relationships at MTPA (i_q is computed through Proportional Integral (PI) controller, i_d as a function of i_q, speed and other parameters).

2.3.2 Control Schemes Based on Biquadratic Torque Equation

As explained in Section 3.1, maximizing the torque equation subject to $i_q^2+i_d^2$ gives necessary i_q, i_d pairs for the MTPA trajectory for a particular motor. Several methods have been proposed based on the solution of the biquadratic equation obtained by differentiating the torque equation with respect to stator current magnitudes [4][28][31]. Since it is computationally intensive to solve the equation in real time, most of the work in the literature proposed using pre-computed look up tables or estimation polynomials. Offline optimization is performed and either stored in the look up tables or curve fit into equations.

Neumann proposed computing the i_q, i_d as a function of normalized torque in [27]. Current components are computed without considering the effects of the magnetic saturation. At higher current levels, magnetic saturation reduces the flux at the air gap and quadrature axis inductance L_q significantly. The nonlinear saturation along with rotor saliency makes it complicated to find optimum i_q, i_d pairs at high current.

A control strategy using the derivative of the torque equation based on constant motor parameters was proposed in [4]. Since the proposed method requires solving a fourth order equation, an offline solution was proposed using the least square estimation method. The proposed least square estimation method provides the current reference as a second order function of the quantity called 'virtual control' which is a scaled version of the required torque.

Authors in [28] proposed using real time implementation of the biquadratic equation solution method based on a constant parameter motor model with a systematic approach proposed by Ferrari [29]. The method provides a solution for the reference current instead of using an iterative search which made it possible to be adopted for online implementation. A recursive method was also proposed in [28] to incorporate inductance variation due to core saturation.

Lorenz proposed offline parameter estimation and a-priori computed an MTPA locus in [30], where the offline estimator is used to produce the MTPA trajectory considering parameter variations. The computed trajectory was different from the one obtained using the constant parameter model; especially at higher current regions. The method also proposed online estimation of motor inductances which were only used to generate a reference voltage for current regulation.

A lookup table based solution was proposed in [31] that considers the effects of the temperature variation as well. Kim proposed generating of two 2-D lookup tables for two different permanent magnet flux linkage conditions ϕ_{M1} and ϕ_{M2}. A flux observer was proposed to estimate permanent magnet flux linkage $\hat{\phi_M}$. Final reference currents were computed by performing interpolation between values found from pre-computed lookup tables for ϕ_{M1} and ϕ_{M2} and estimated flux linkage $\hat{\phi_M}$.

Lorem ipsum dolor sit amet, consetetur sadipscing elitr, sed diam nonumy eirmod tempor invidunt ut labore et dolore magna aliquyam erat, sed diam voluptua. At vero eos et accusam et justo duo dolores et ea rebum. At vero eos et accusam et justo duo dolores et ea rebum. At vero eos et accusam et justo duo dolores et ea rebum.

2.3.3 Control Schemes Based on id, iq Relationship at MTPA

Instead of finding id, iq using polynomials or look up tables, several researchers proposed using the id, iq relationship for MTPA. In these methods, only id was generated as functions of iq, speed and other parameters. A PI controller or some other means were used to generate iq reference.

Morimoto proposed computing the required id based on equations found by differentiating the torque expression with respect to current magnitude [32]. This gave following straight forward relationship between id and iq:

$$\mathrm{i}_d = \frac{\Phi_M}{2(L_d - L_q)} - \sqrt{\frac{{\Phi_M}^2}{4\left(L_d - L_q\right)^2} + {\mathrm{i}_q}^2} \tag{2.3}$$

id can be represented by the stator current i_s:

$$\mathrm{i}_d = \frac{\Phi_M}{2(L_d - L_q)} - \sqrt{\frac{{\Phi_M}^2}{4\left(L_d - L_q\right)^2} + \frac{{\mathrm{i}_s}^2}{2}} \tag{2.4}$$

where $\mathrm{i}_s = \sqrt{{\mathrm{i}_d}^2 + {\mathrm{i}_q}^2}$.

In the proposed algorithm, a PI speed controller was used to generate the necessary i_q based on the operating conditions. The required i_d for MTPA operation was generated using equation 2.4. Introduction of the computed i_d changes the operating point while the PI controller adjusts the i_q reference that in turns produces a new id reference. The procedure ultimately converges to a suitable i_d, i_q pair. An almost similar technique was proposed by the same authors in [33] which considers Lq as a function of iq to compensate for magnetic saturation.

Niazi and Toliyat proposed online estimation of L_d, L_q and utilized the estimated parameters while computing the reference currents [10]. A steady state motor model was used for parameter estimation. This method was proposed for permanent magnet assisted synchronous reluctance motors that has a similar torque equation as IPMSMs. The i_d, i_q relationship mentioned in equation 2.5 provides another convenient form of solution based on current phase angle β in a straight forward manner [35].

$$\beta = sin^{-1}\left(\frac{-\phi_M + \sqrt{{\phi_M}^2 + 8\left(L_d - {L_q}^2\right){\mathrm{i}_s}^2}}{4\left(L_d - L_q\right)\mathrm{i}_s}\right) \tag{2.5}$$

$$\mathrm{i}_d = \frac{\phi_M}{2(L_d - L_q)} - \sqrt{\frac{{\phi_M}^2}{4\left(L_d - L_q\right)^2} + {\mathrm{i}_q}^2} \tag{2.6}$$

Equation 2.5 was used with the estimated L_d, L_q along with some perturbation technique for maximizing torque generation. An almost similar strategy was also proposed in [36], but modifications were made in the parameter estimation technique. An affine projection algorithm [37] was proposed for parameter estimation which required fewer computations compared to Recursive Least Square or Kalman filtering techniques.

Kang, Lim et al. proposed a method based on offline training of the motor at constant temperature to develop a lookup table of reference current magnitudes and phase angles for operating at MTPA [38]. The novelty of the method was mostly on adding the temperature compensation considering the weakening of permanent magnets at high temperature. A reverse lookup table was used for torque estimation in the proposed method. The magnetic flux linkage was modeled using the reversible temperature coefficient of the permanent magnet material.

Modeling id as a function of $iq$and speed was proposed in [39] by Mademlis, Kioskeridis, et al. Instead of using the equation based on MTPA, a loss modeling control (LMC) was proposed. The control scheme proposes determination of optimum id using a predetermined polynomial of speed and iq.

2.3.4 Control Methods Based on Search Algorithm

Another well-known technique involves using some online search algorithm for achieving MTPA operation. The benefit of using such an approach is to get lower parameter dependence. Even an ill-defined motor model can give satisfactory performance because of lower dependence on the motor model. The downside of these algorithms is poor performance during transients. Most of the search algorithms rely on some means of perturb and observe method which takes time to converge to a desired operating point. Moreover, Mademlis, Kioskeridis et al demanded that, algorithms based on searching sometimes fail to attain a desired state and cause undesirable torque disturbance [39].

Among different search based algorithms proposed for PM motors, Colby and Novotny proposed a technique in [40] which only requires DC link current measurement. Instead of going into the DQ reference frame, a method was proposed which implements the control in the 3-phase abc reference frame. In the proposed method, DC link current is used to generate an optimum voltage reference to minimize losses.

Zhu, Chen and Howe in [5] proposed searching for optimum id, iq by monitoring the real time performance of the motor. The amount of id is controlled by measuring the error between the actual and the reference current in the flux weakening region. During MTPA operation, the id command is generated by observing the current phasor magnitude or from DC link current measurement. While the speed remains constant, a change in the DC link current is used to determine the performance of the machine and adjust the id command.

On the other hand, authors in [9] and [41] proposed an online tracking method to determine optimum current phase angle β for MTPA operation. Anton in [9] proposed estimation of β by observetion method to minimize the magnitude of the stator current.

At MTPA point, β would be oscillating around its optimum value. The proposed technique performs well at steady state but would fail during rapid load and speed command changes. Kim in [41] proposed a method that would bring the $\delta T/\delta\beta$ to zero at MTPA point through high frequency current injection.

Bolognani proposed a hybrid controller which uses pre-computed current phase angle β for MTPA operation using a constant parameter motor model [42]. A new reference frame was proposed called the MTPA reference frame which is essentially the dq reference frame shifted by the current phasor angle β. The phase shifting of the reference frame caused only iq ˆ to produce torque. An algorithm to modify precomputed β was only introduced at steady state as a compensation for parameter variation.

3. BURIED MAGNET MOTORS

3.1 Introduction to IPMSM

The PMSM is a synchronous AC motor, normally with a three phase stator winding similar to induction motors. The rotor however, is different. Permanent magnets provides a constant flux to magnetize the motor. The lack of an electrical magnetization system gives the advantage of a more energy efficient motor.

Depending of the armature winding distribution the PMSM can be di- vided into two types, Brushless DC (BLDC) or Permanent Magnet AC (PMAC) motors. The PMAC motor has armature winding that spans close to 180◦ electrical degrees, which gives the motor a sinusoidal back EMF. This is the motor type that this thesis will focus on. The BLDC has armature windings that spans over a smaller angle, which gives the motor a trapezoidal shaped back EMF.

The PMSM is normally controlled with a frequency converter that sup- plies the motor with the correct frequency and voltage/current values.

3.2 Rotor Designs

There are many possible design choices for the rotor, some of them can be seen in Figure 3.1. Magnets can be mounted on the surface, in the surface and under the surface, all with different advantages/disadvantages. Surface mounted magnets will not withstand high rotational speed due to high centrifugal forces which crack or separates the magnets from the rotor. Subsurface- or buried- magnets need to be insulated from each other with slots or non magnetic material to avoid a magnetic short circuit, but the magnets are protected and held into place at high speeds. Figure 3.1a, 3.1b, 3.1e, 3.1f & 3.1i show rotors with buried magnets.

Figure 3.1a and 2.1f show rotors with damper windings, the winding provides a possibility for asynchronous starting and dampens oscillations.

Figure 3.1g and 3.1h show rotors with rounded magnets, which gives a more sinusoidal field distribution with less harmonics [3].

A rotor with surface magnets has a wide magnetic air gap, resulting in a low magnetizing inductance and difficulty to affect the machines electromag- netic properties by controlling the stator current. With buried magnets the air gap can be smaller and the magnetizing inductance higher, increasing the controllability of the magnetic properties caused by the stator current. This gives the motor a possibility to extend its speed range by reducing the flux, so called flux weakening operation.

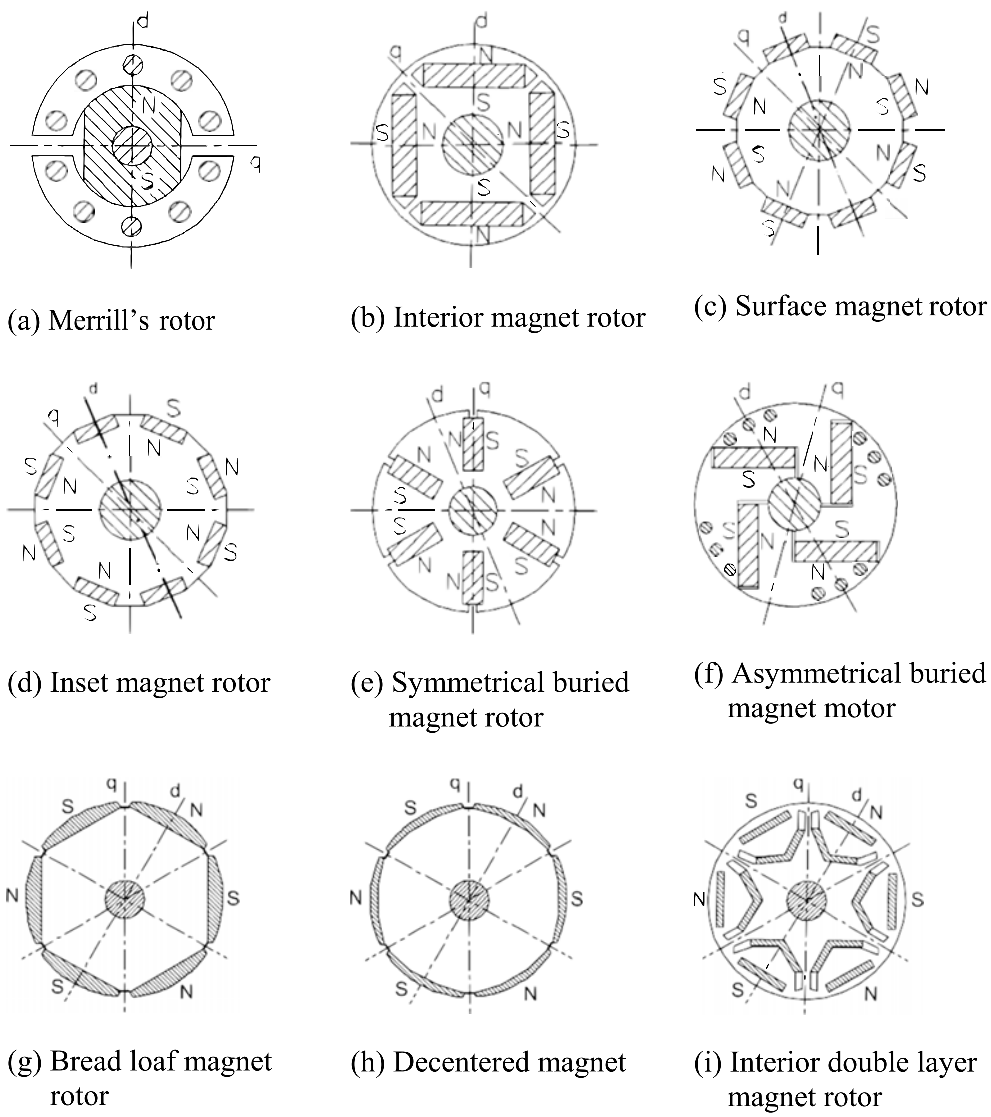

(a) Merrill's rotor
(b) Interior magnet rotor
(c) Surface magnet rotor
(d) Inset magnet rotor
(e) Symmetrical buried magnet rotor
(f) Asymmetrical buried magnet motor
(g) Bread loaf magnet rotor
(h) Decentered magnet
(i) Interior double layer magnet rotor

Figure 3.1: Different types of rotor configurations.

3.3 Definition of Saliency

Saliency is a measure of the non-symmetry of the motors magnetic properties. The non-symmetry occur by the difference in the reluctance path between the rotor and stator. This difference comes from variations of the rotors geometry or material, and a difference can be seen in the motors induction parameters Ld and Lq. Three different types of saliencies can exist, non-, positive or negative salient.

It doesn't seem to be any consensus about naming different saliency rotor types, does NS stands for Normal Saliency or Negative Saliency? And what does Normal, Negative, Positive and Inverse means in terms of saliency? Some thinks Inverse Saliency is the opposite compared with a traditional buried magnet rotor (Ld < Lq), while other think that Inverse Saliency is the opposite of an electrically excited synchronous rotor (Ld > Lq).

To complicate things further a round rotor with magnets attached to the surface will physically look as if it would be salient (see Figure1 3.1), but it doesn't have any saliency at all because the magnets permeability is almost the same as air and will not affect the reluctance path.

Table 3.1: Different conventions of naming of salient machines.

	$Ld > Lq$	$Ld < Lq$
Bianchi[4]	Normal	Inverse
Mancado[5]	Inverse	Normal
Mancado[6]	Negative	Positive
Kronberg	Positive	Negative

The author's definition of saliency is based on the traditional electrically excited synchronous machine and its magnetic properties, this will be referred as Positive Saliency.

- SPMSM - Surface mounted Permanent Magnet Synchronous Motor. Rotor type without any saliency, equal reluctance along the rotor circumference.
- NSPMSM - Negative Saliency Permanent Magnet Synchronous Motor. Rotor type with lower reluctance between the poles.
- PSPMSM - Positive Saliency Permanent Magnet Synchronous Motor. Rotor type with lower reluctance at the poles.

4. MATHEMATICAL ANALYSIS

4.1 Introduction to Control Theory of IPMSM

A three phase PMSM is normally constructed with sinusoidally distributed phase windings, with a 120° phase shift between the three windings. In a stator reference frame coordinate system the phase vectors A, B, C can be seen as they are fixed in angle, but with time varying amplitudes. This three vector representation makes calculation of machine parameters unnecessarily complex. By transforming the system into a two vector orthogonal system, the necessary calculations could be much simpler.

4.2 Transformations

A three phase machine can be described by a set of differential equations with time dependent coefficients. By transforming the motor parameters, the complexity of machine calculations can be reduced. The most common methods to do this are the Clarke and Park transformations.

According to the definitions the transforms give a third component, 0 or zero-sequence. But since a motor normally is a balanced load, the zero- sequence can be ignored.

The two transformations presented below are not the original Clarke and Park, but in a slightly modified form to make them power invariant [9]. By using these modifications it is possible to calculate the correct power/- torque values from the transformed motor parameters without the need to transform them back to three phase values.

4.2.1 Clarke's Transformation

The Clarke transformation changes a three phase system into at two phase system with orthogonal axes in the same stationary reference frame. The new two phase variables are denoted α and β, the original and transformed system can be seen in Figure 4.1a.

The ABC parameters are transformed into αβ0 parameters by equation 4.1, and in reverse by equation 4.2 [10].

$$f_{\alpha\beta 0} = T\, f_{ABC} \tag{4.1}$$

$$f_{ABC} = T^{-1} f_{\alpha\beta 0} \tag{4.2}$$

Where f can be any one of the motors armature parameters, and the transformation matrix T is.

$$T = \sqrt{\frac{2}{3}} \begin{bmatrix} 1 & -\frac{1}{2} & -\frac{1}{2} \\ 0 & \frac{\sqrt{3}}{2} & -\frac{\sqrt{3}}{2} \\ \frac{1}{\sqrt{2}} & \frac{1}{\sqrt{2}} & \frac{1}{\sqrt{2}} \end{bmatrix} \tag{4.3}$$

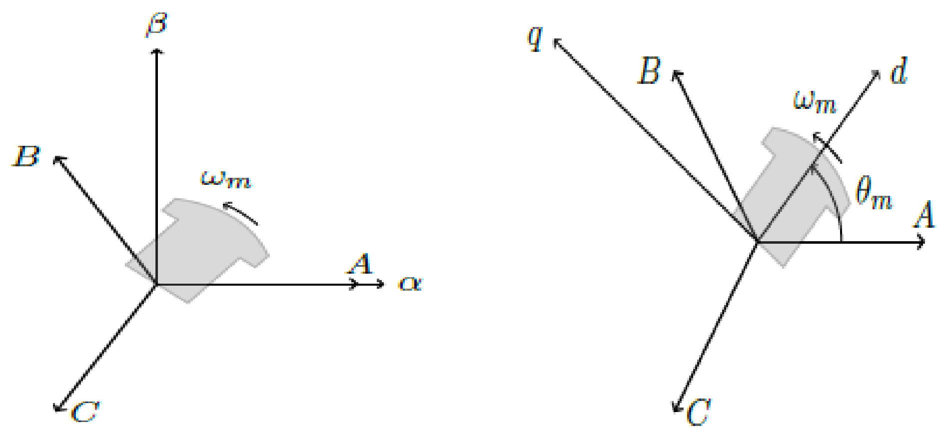

(a) ABC to αβ (b) ABC to dq

Figure 4.1: Clarke and Park transform

4.2.2 Park's Transformation

The Park transformation changes a three phase system in one stationary reference frame into a two phase system with orthogonal axes in a different rotating reference frame. The two new phase variables are denoted d and q, and are referred to as the motors direct- and quadrature-axis. The original and transformed system can be seen in Figure 4.1b. The ABC parameters are transformed into dq0 parameters by equation 4.4, and in reverse by equation 4.5 [10].

$$f_{\alpha\beta 0} = T\, f_{ABC} \tag{4.4}$$

$$f_{ABC} = T^{-1} f_{\alpha\beta 0} \tag{4.5}$$

Where f can be any one of the motors armature parameters, and the transformation matrix T is.

$$T = \sqrt{\frac{2}{3}} \begin{bmatrix} \cos(\theta_m) & \cos\left(\theta_m - \frac{2\,\pi}{3}\right) & \cos\left(\theta_m + \frac{2\,\pi}{3}\right) \\ \sin(\theta_m) & \sin\left(\theta_m - \frac{2\,\pi}{3}\right) & \sin\left(\theta_m + \frac{2\,\pi}{3}\right) \\ \frac{1}{\sqrt{2}} & \frac{1}{\sqrt{2}} & \frac{1}{\sqrt{2}} \end{bmatrix} \tag{4.6}$$

By using the Park's transform, the stator parameters such as voltages, cur- rents, and flux linkages, are associated with fictitious stator windings that rotate with the rotor. The time varying parameters between stator and rotor are thus eliminated and all variables are expressed in the same orthogonal or mutually decoupled direct- and quadrature-axes.

4.3 Motor Equations in the Rotor Reference Frame

After the described transformation the different parameters in a synchronous machine can be described by the following equations. Flux linkages below are described in equations 4.11 through 4.14:

$$v_{sd} = R_s i_{sd} + \frac{d\lambda_{sd}}{dt} - \omega_e \lambda_{sq} \tag{4.7}$$

$$v_{sq} = R_s i_{sq} + \frac{d\lambda_{sq}}{dt} - \omega_e \lambda_{sd} \tag{4.8}$$

$$v_D = R_D i_D + \frac{d\lambda_D}{dt} = 0 \quad \textbf{(4.9)}$$

$$v_Q = R_Q i_Q + \frac{d\lambda_Q}{dt} = 0 \quad \textbf{(4.10)}$$

$$\lambda_{sd} = (L_{md} + L_{s\sigma}) + L_{md} i_D + \lambda_{pm} = L_{sd} i_{sd} + L_{md} i_D + \lambda_{pm} \quad \textbf{(4.11)}$$

$$\lambda_{sq} = \left(L_{mq} + L_{s\sigma}\right) + L_{mq} i_Q = L_{sq} i_{sq} + L_{mq} i_Q + \lambda_{pm} \quad \textbf{(4.12)}$$

$$\lambda_D = L_{md} i_{sd} + L_D i_D + \lambda_{pm} \quad \textbf{(4.13)}$$

$$\lambda_Q = L_{mq} i_{sq} + L_Q i_Q \quad \textbf{(4.14)}$$

By describing the Permanent Magnet as a current source, the flux linkage λ_{pm} can be seen as:

$$\lambda_{pm} = L_{md} i_{pm} \quad \textbf{(4.15)}$$

The subscripts d and q denotes if the component is along the direct or quadrature axes, and; v_{sd} and v_{sq} are the terminal voltage components. v_D and v_Q are the induced voltage in the damper windings and can be considered to be zero at steady state. i_{sd} and i_{sq} are the armature winding current components. L_{sd} and L_{sq} are the armature self-inductances components. $L_{s\sigma}$ is the stator leakage inductance. R_s is the armature winding resistance. λ_{pm} is the flux linkage per phase generated from the excitation system. R_D and R_Q are the damper windings resistance. L_D and L_Q are the damper windings self-inductance.

Instantaneous power in ABC reference system is defined as:

$$P_{in,abc} = v_a i_a + v_b i_b + v_c i_c \quad \textbf{(4.16)}$$

Using the above transformation it is expressed in dq0 domain as:

$$P_{in,dq} = \frac{3}{2}(v_d i_d + v_q i_q) + 3v_0 i_0 P_{in,abc} = v_a i_a + v_b i_b + v_c i_c \quad \textbf{(4.17)}$$

Ignoring zero sequence and inserting equations 4.7 and 4.8 into the above, we get:

$$P_{in,dq} = \omega_e \frac{3}{2}\left(\lambda_{sd} i_{sq} - \lambda_{sq} i_{sd}\right) + \frac{3}{2}(R_s {i_{sd}}^2 + \frac{d\lambda_{sd}}{dt} i_{sd} + R_s {i_{sq}}^2 + \frac{d\lambda_{sq}}{dt} i_{sq}) \quad \textbf{(4.18)}$$

Where the first term accounts for the electromagnetic power and ω_e is the electrical angular frequency. The mechanical angular frequency can be expressed as: $\omega_e = \frac{p}{2}\omega_m$ where p is the number of poles. Assuming steady state, the electromagnetic power P_e can be expressed as:

$$P_e = \omega_m \frac{3}{2}\frac{p}{2}\left(\lambda_{sd} i_{sq} - \lambda_{sq} i_{sd}\right) \quad \textbf{(4.19)}$$

Divide the power with rotational speed ω_m to get the motors electromechanical torque T_e and replace the flux linkages λ_{sd} and λ_{sq} with equations 4.11 and 4.12, to get the following equation:

$$T_e = \frac{3}{2}\frac{p}{2}[\left(L_{sd} i_{sd} + \lambda_{pm}\right) i_{sq} - L_{sq} i_{sq} i_{sd}] \quad \textbf{(4.20)}$$

4.4 The Permanent Magnet Synchronous Machine Equivalent Circuits and Mechanical Motor Model

To be able to simulate the electrical behavior of the motor in any electrical circuit analysis program the motors equivalent circuit (Figure 4.2 and 4.3) is needed. By transforming the drive voltage into DQ parameters and connecting it to its respective DQ equivalent circuit, measurement of the models currents can be done.

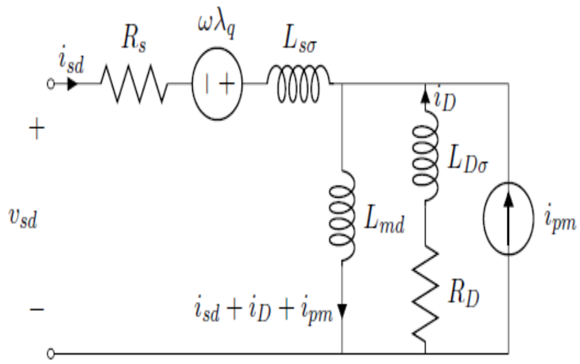

Figure 4.2: Equivalent circuit for a salient machines direct axis.

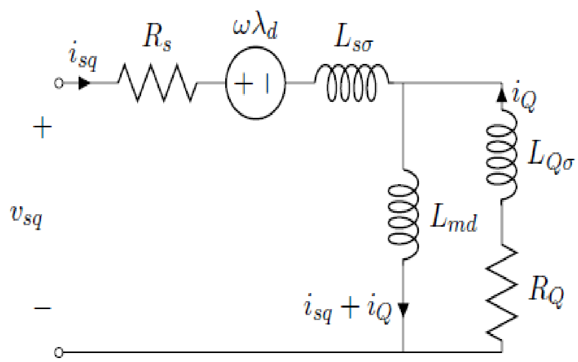

Figure 4.3: Equivalent circuit for a salient machines quadrature axis.

From the current values the motors torque can be calculated and the speed can be calculated from the following equation:

$$\frac{p}{2}(T_e - T_L) = J\frac{d\omega_r}{dt} \tag{4.21}$$

Where T_L is the load torque, ω_r is the rotational speed and J is the motor and loads inertia. With the above parameters it is possible to implement a model of a PMSM in a circuit simulation software. However, in this thesis a Simulink model has been used.

5. CONTROL THEORY

5.1 Introduction to Control Methods

Synchronous motors have to be driven by a Variable Frequency Drive (VFD) to be able to run at different speeds. Control methods for electric motors can be divided into two main categories depending of what quantities they control. The control algorithm Scalar Control controls only magnitudes, whereas the algorithms Vector Control controls both magnitude and angles. These two main methods can be further divided into a number of different methods depending of their functionality, an overview over different control methods can be seen in Figure 5.1.

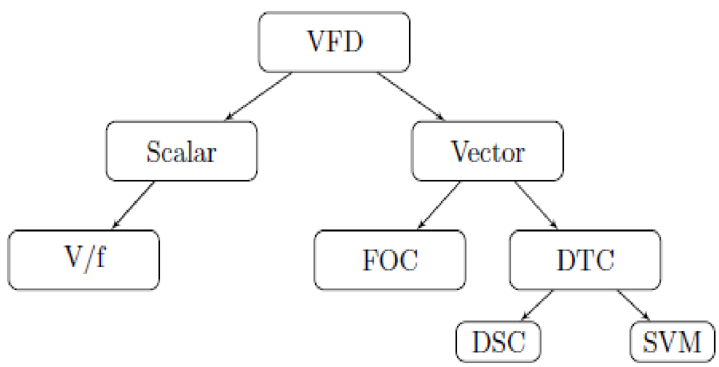

Figure 5.1: Overview of available control strategies.

5.2 Scalar Control

The simplest method to control a PMSM is scalar control, where the relationship between voltage, current and frequency are kept constant through the motors speed range. The frequency is set according to the wanted synchronous speed and the magnitude of the voltage/current is adjusted to keep the ratio between then constant. No control over angles is utilized, hence the name scalar control. The method uses an open-loop control approach without any feedback of motor parameters or its position. This makes the method easy to implement and with low demands on computation power of the control hardware, but its simplicity also comes with some disadvantages. One of them are instability of the drive system after exceeding a certain applied frequency, to overcome this the rotor has to be constructed with damper windings to assure synchronization of the rotor to the electrical frequency [11]. This will limit the number of design choices for the rotor, e.g. the magnets has to be located on the inside of the damper bars. Most PMSM are therefore constructed without damper windings, and they are not suitable for traditional scalar control.

Another drawback with the lack of feedback is the systems low dynamic performance, which limits the use of this control method to e.g. fan- and pump-drives [11]. For applications that demands high dynamic performance, vector control is recommended. One way to improve the performance without the use of position feedback is to use the variations in the inverters DC link voltage to determine the correct modulation [12] [13].

5.3 Vector Control

With control of both magnitude and the angle of the flux it is possible to achieve higher dynamic performance of the drive system than scalar control can offer. Two different types of strategies exist for vector control, Field Oriented Control and Direct Torque Control.

5.3.1 Field Oriented Control (FOC)

The concept of FOC was first invented in the beginning of 1970s [53]. This method brought forward intensive efforts in investigating high performance control of ac drives because of the fact that an induction motor controlled by an FOC method/algorithm can be controlled in a similar manner to the control of a separately excited dc motor [18]. Such FOC is also known as vector control, decoupling control, and orthogonal control [18]. In general, the principle of FOC schemes implies independent (decoupled) control of flux – current and torque – current components of a stator current through a coordinated change in the supply voltage amplitude, phase angle and frequency. As the flux variation tends to be slow, especially with current control, constancy of flux should produce a fast torque response, and consequently reasonable speed response [50].

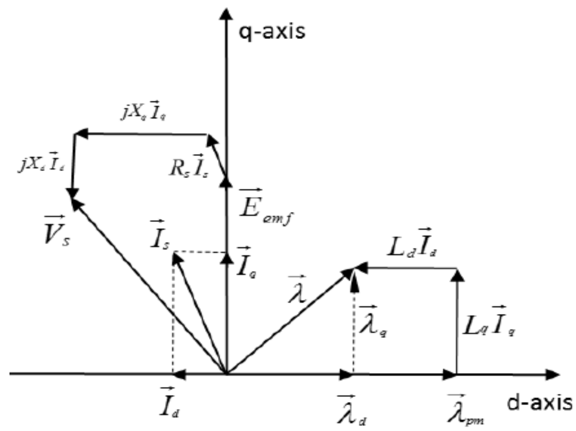

Figure 5.2: Phasor diagram of a PMSM in d-q frame.

The fundamental objective of most FOC algorithms is to control the amplitude, phase, and frequency of stator flux linkages. This objective can be achieved by controlling the stator current phasor, I_s as shown in Figure 5.2. In terms of phasor components as shown in Figure 5.2, the voltage equation can be expressed as follows:

$$V_s = E_{emf} + R_s i_s + jX_d i_d + jX_q i_q \quad \textbf{(5.1)}$$

Where, V_s is the stator phase voltage, E_{emf} is the back-EMF in a PM motor, i_s is the stator current phasor, and X_d and X_q are the DQ axes reactances. The value of the back-EMF, $Eemf$, can be calculated from the flux linkage due to the permanent magnet, λ_{pm}, as follows:

$$E_{emf} = \omega_e \lambda_{pm} \quad \textbf{(5.2)}$$

Notice, in the phasor diagram of Figure 5.2, voltages, currents and flux linkages are in RMS values.

To illustrate how the FOC method controls the motor in a motor-drive system, a general control structure is presented in Figure 5.3 for a better demonstration. There are two loops in the control scheme of Figure 5.3: the inner current loop and the outer speed loop. Normally, the current loop is used to obtain a desired torque. Meanwhile, the speed loop assures that the actual speed follows the commanded speed.

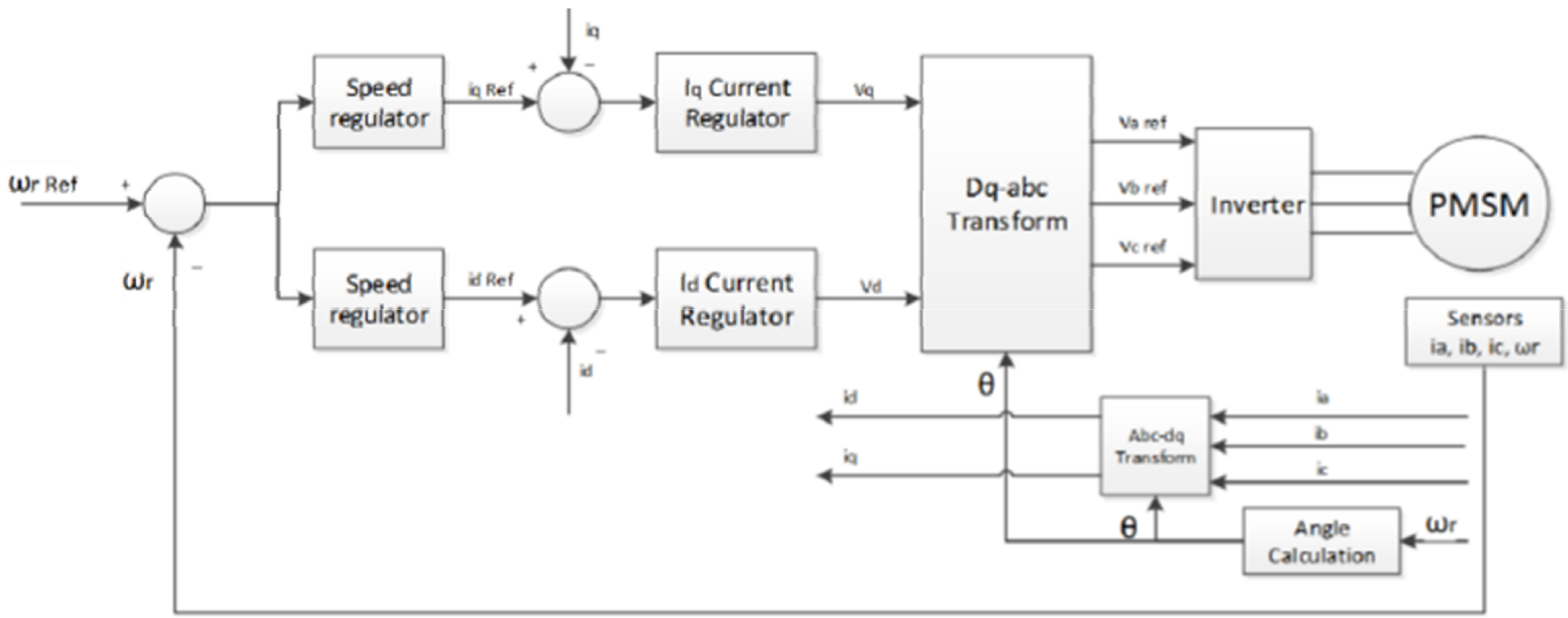

Figure 5.3: General control scheme of the Field Oriented Control.

In most controller designs related to FOC logic structure, control algorithms are embedded in the speed regulator portion of the speed loop. Thus, the design of the speed regulator could be simple or complex according to the various FOC algorithms. Notice that there is no reference torque that can be found in Figure 5.3. This does not mean that the torque is not controlled. In fact, a reference torque can be generated by the speed regulator. Then, current references can be obtained according to this commanded reference torque. Moreover, torque feedback can also be added into the speed regulator through a torque transducer, not shown in Figure 5.3. To avoid complexities, the general speed regulator can be decomposed into the speed regulator which gives the torque reference, and the torque regulator which produces the current reference. In general, the speed regulator is the main controller in most FOC logic structures. As to the inner- loop controller, the current regulator assures that the current follows its reference value which is the output of the speed regulator. The design of the current regulator usually depends on motor parameters. While, the design of the speed regulator is usually based on the nature of the control algorithms.

In conventional FOC categories, there are several control algorithms/strategies, which, namely, are the MTPA strategy, the FW strategy, unity power factor control, and optimal efficiency control, etc. [18-20]. For traction applications, the MTPA control is the most effective strategy in the low speed regions. While, the FW control is necessary in high speed applications. Although MTPA and FW employ different algorithms, they are FOC methods in their nature.

5.3.2 Direct Torque Control (DTC)

Direct Torque Control was first introduced for induction motors (IM) by Takahashi and Noguchi [16] in 1984 and the Direct Self Control method by Depenbrock [17] in 1985. The methods were characterized by their simplicity, good performance and robustness. Unlike the FOC method, DTC worked without any external measurement of the rotors mechanical position. However, to ensure correct rotational direction of a PMSM, the rotor position shall be known at motor start up. The reason behind the simplicity is that DTC not require any current regulators, transformations to rotating reference frame or PWM generators.

The disadvantages are, difficulty to control torque at low speed, high current and torque ripple, variable switching frequency, high noise level at low speed and lack of direct current control. It is also important to do a correct estimation of the dc-link voltage and stator resistance to get stability of the drive system [18].

There are a number of different suggestions for improving the characteristics of DTC, such as.

- Improved switching tables and increasing the number of sectors [19] [20].
- Using multilevel hysteresis comparators [20].
- Fixed frequency switching with PWM or Space Vector Modulation (SVM) [20] [21]

The working principle for the basic DTC is to select a voltage vector based on the error between requested and actual values of torque and flux linkage, it also uses a ruff position estimation that divides one electrical revolution into six sectors depending on the flux linkage angle. A basic scheme for DTC can be seen in Figure 5.4, the different blocks are described below [22].

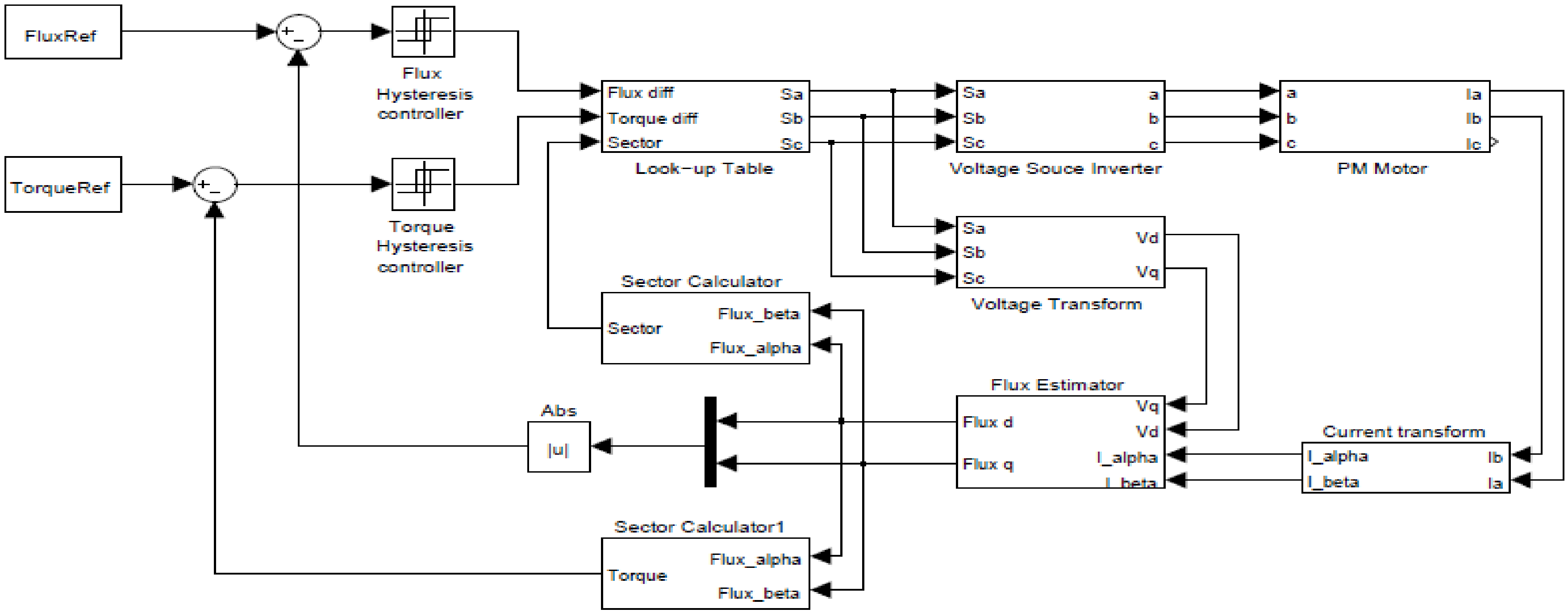

Figure 5.4: DTC control layout.

5.3.3 Maximum Torque per Ampere (MTPA) Control Algorithm

In order to produce the maximum torque at a given current value, the torque expression for PM motors has to be analyzed. For SPM motors, which have no saliency, the reluctance torque is zero. Thus, for SPM motors, the torque expression can be rewritten as follows [25]:

$$T_e = \frac{3}{2}\frac{p}{2}\lambda_{pm} i_q \tag{5.3}$$

Keeping $i_q = I_s$ and $i_d = 0$, it is the most convenient approach to control an inverter-fed SPM motor in order to produce the maximum torque.

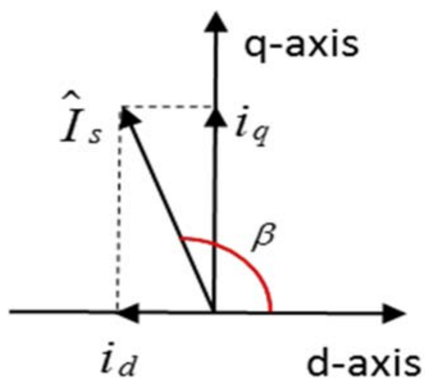

Figure 5.5: Torque angle.

Since IPM motors have larger q-axis reactance/inductance than d-axis reactance/inductance that is $L_q > L_d$, the reluctance torque is present. Therefore, the maximum torque becomes a combination of the magnet excitation torque and the reluctance torque. From the Figure 5.5, we can write:

$$i_d = i_s \cos(\beta) \quad \&\& \quad i_q = i_s \sin(\beta) \tag{5.4}$$

where, is is the amplitude of the stator phase current of an IPM motor, and β ($180° > \beta \geq 0°$) is defined as the "torque angle", which is the angle between the stator phase current vector and the positive direction of the d-axis as shown in Figure 5.5.

By substituting above current equations into torque equation, one can obtain the following:

$$T_e = \frac{3}{2}\frac{p}{2}(\lambda_{pm} i_s \sin(\beta) + (L_d - L_q) i_s{}^2 \frac{\sin(2\beta)}{2}) \qquad \textbf{(5.5)}$$

As aforementioned earlier, the developed torque can be seen as a combination of the magnet excitation torque, T_{mag}, and the reluctance torque, T_{rel}, which can be expressed as follows:

$$T_e = T_{mag} + T_{rel} \qquad \textbf{(5.6)}$$

$$T_{mag} = \frac{3}{2}\frac{p}{2}\lambda_{pm} i_s \sin(\beta) \qquad \textbf{(5.7)}$$

$$T_{rel} = \frac{3}{2}\frac{p}{2}(L_d - L_q) i_s{}^2 \frac{\sin(2\beta)}{2} \qquad \textbf{(5.8)}$$

As the torque angle, β, changes, the variation of the magnet excitation torque and the reluctance torque can be seen in Figure 5.6:

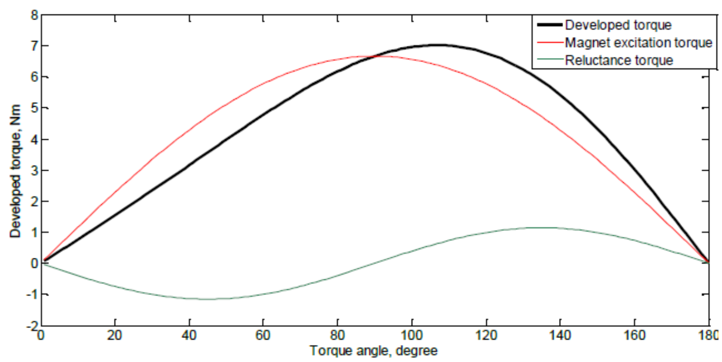

Figure 5.6: Developed torque vs. torque angle of IPM motors.

As shown in Figure 5.6, the torque angle corresponding to the maximum magnet excitation torque does not provide the maximum developed torque. Since SPM motors don't have any significant reluctance torque component, the magnet excitation torque and the developed torque are equal in SPM motors. Therefore, this also implies that IPM motors have higher maximum developed torque than SPM motors. Therefore, this also implies that IPM motors have higher maximum developed torque than SPM motors. The torque angle which results in the maximum torque of IPM motors can be derived by setting the derivative of the torque in equation 5.8 to zero, which can be expressed as follows:

$$\frac{dT_e}{d\beta} = \frac{3}{2}\frac{p}{2}(\lambda_{pm} I_s \cos\beta + (L_d - L_q) I_s^{\,2} \cos 2\beta) \tag{5.9}$$

For further simplicity, equation 5.9 can be rewritten as follows:

$$\lambda_{pm}(I_s \cos\beta) + (L_d - L_q)((I_s \cos\beta)^2 - (I_s \sin\beta)^2) = 0 \tag{5.10}$$

Afterwards one can obtain:

$$\lambda_{pm} i_d + (L_d - L_q)(i_d^{\,2} - i_q^{\,2}) = 0 \tag{5.11}$$

Since $(i_d^{\,2} - i_q^{\,2}) = I_s^{\,2}$ it follows that i_q can be expressed as follows:

$$i_q = \sqrt{I_s^{\,2} - i_d^{\,2}} \tag{5.12}$$

By substituting equation 5.12 into equation 5.11, a binominal equation of d-axis current can be written as follows:

$$2(L_d - L_q) i_d^{\,2} + \lambda_{pm} i_d - (L_d - L_q) I_s^{\,2} = 0 \tag{5.13}$$

From equation 5.13, two solutions can be obtained as follows:

$$i_{d1} = \frac{\lambda_{pm} + \sqrt{\lambda_{pm}^{\,2} + 8(L_d - L_q)^2 I_s^{\,2}}}{4(L_d - L_q)} \tag{5.14}$$

$$i_{d1} = \frac{\lambda_{pm} - \sqrt{\lambda_{pm}^{\,2} + 8(L_d - L_q)^2 I_s^{\,2}}}{4(L_d - L_q)} \tag{5.15}$$

Since IPM motors have larger L_q than L_d , to obtain a positive reluctance torque, one has to keep the torque angle larger than 90°, which can be obtained from equation 5.8. Therefore, the projection of I_s on the d-axis should have a negative value due to such torque angle, which also indicates that i_{d2} in equation 5.15 is the expected useful solution. From the above, the d- and q-axis currents for MTPA control of IPM motors can be expressed as follows:

$$i_{dm} = \frac{\lambda_{pm} - \sqrt{\lambda_{pm}{}^2 + 8(L_d - L_q)^2 I_s{}^2}}{4(L_d - L_q)} \quad \textbf{(5.16)}$$

$$i_{qm} = \sqrt{I_s{}^2 - i_{dm}{}^2} \quad \textbf{(5.17)}$$

Here, the torque angle, β, for this maximum torque condition is hence obtained as follows:

$$\beta_m = \arctan(\frac{i_{qm}}{i_{dm}}) \quad \textbf{(5.18)}$$

Although voltage constraints are not taken into consideration in the MTPA control, the developed torque is limited by supply current. For each supply current value, there is a particular pair of d-axis current and q-axis current that results in the maximum torque under that condition. Therefore, the torque angle for the MTPA operation is determined not only by motor parameters but also by supply current value. For different supply currents, there are different cross points between the current circles and the MTPA trajectory as shown in Figure 5.7, which yields different torque angles for MTPA operations.

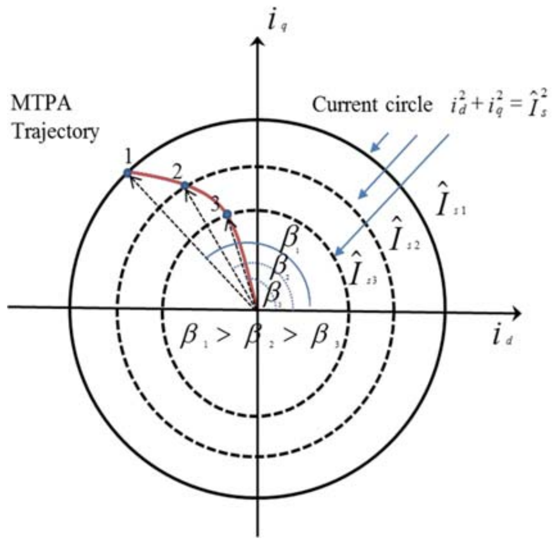

Figure 5.7: The MTPA trajectory for IPM motors

5.3.4 Flux-Weakening Control Algorithms

For traction applications in Evs, PMSM-drive systems normally require a wide constant power speed range (CPSR). However, a specific power inverter cannot drive PMSMs at high speeds because of the fact that the back-EMF is proportional to motor speed and air gap flux, thus, leading to higher back-EMF values. Once the back-EMF becomes larger than the maximum output voltage of the drive, the PMSM will be incapable of drawing current and hence incapable of developing torque. Thus, when the back-EMF reaches the voltage threshold of a drive, the rotor speed of such a motor cannot be increased unless the air gap flux can be weakened. Considering that the rotor magnetic field generated by the PMs can only be weakened indirectly through armature MMF demagnetization of the PMs, and hence, an extended speed range can be achieved by means of FW control. During the FW operation region, a demagnetizing MMF is established by the stator currents and winding to counteract the “apparent” MMF established by PMs mounted on the rotor. As a result, the resultant air-gap flux is indirectly reduced/weakened and correspondingly the motor speed is increased [54].

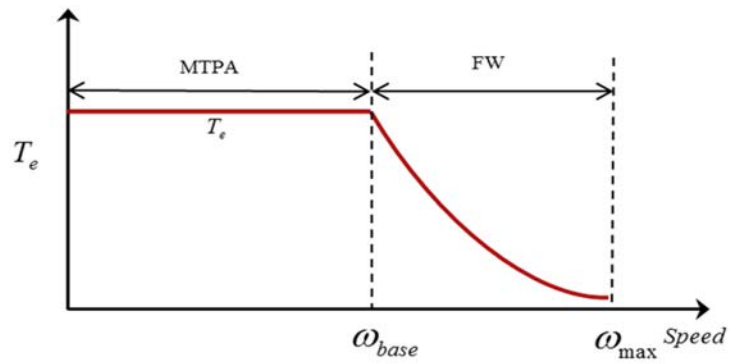

Figure 5.8: Torque vs. speed characteristics of PMSM.

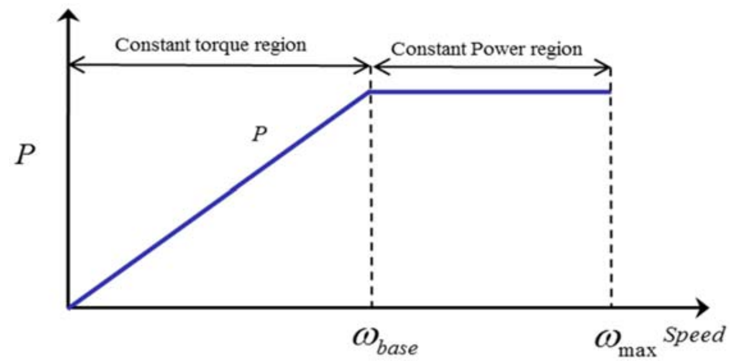

Figure 5.9: Power vs. speed characteristics of PMSM.

Without FW control, the back-EMF of a PM motor will keep increasing with speed. Therefore, the output voltage of the drive for such a PM motor has to be increased to keep desired phase currents. In the constant torque region as shown in Figure 5.8, a motor can be accelerated by the maximum torque until the terminal voltage of such motor reaches its limit value at $\omega_e = \omega_{base}$, which is defined as the base speed or corner speed. Such base speed is the highest speed of a PM motor controlled by the aforementioned MTPA method.

Substituting current equations into voltage equation, one can obtain the following for the space vector of the stator terminal voltage:

$$V_s = \sqrt{(\omega_e L_q i_q)^2 + (\omega_e (L_d i_d + \lambda_{pm}))^2} \quad \textbf{(5.19)}$$

Thus, from equation 5.19 the electrical speed, ω_e, has to satisfy the following expression:

$$\omega_e = \frac{V_s}{\sqrt{(L_d i_d + \lambda_{pm})^2 + (L_q i_q)^2}} \quad \textbf{(5.20)}$$

Hence the base speed, ω_{base}, can be obtained as follows:

$$\omega_{base} = \frac{V_{\max}}{\sqrt{(L_d i_d + \lambda_{pm})^2 + (L_q i_q)^2}} \quad \textbf{(5.21)}$$

where, $V_{\max}$ is the amplitude of the maximum output voltage space vector of a drive, and idm/iqm are the d/q axes currents for the MTPA operation condition.

Normally, for all the FW control algorithms, there are two constraints that should be considered: namely the maximum current and the maximum voltage. Unlike the aforementioned MTPA control, the torque capability in the FW region is determined by both current and voltage limitations. In a motor-drive system, the current limitation is usually decided by the motor side, which depends on a motor's thermal dissipation and cooling means. However, the maximum voltage is typically decided by the drive side, which has a limited dc bus voltage.

The current limitation, $I_{\max}$, which is the amplitude of the maximum phase current, can be drawn as a circle in the d-q frame as shown in Figure 5.10, which can be formulated in the following fashion:

$$i_d^{\,2} + i_q^{\,2} = I_s^{\,2} \le I_{\max}^{\,2} \quad \textbf{(5.21)}$$

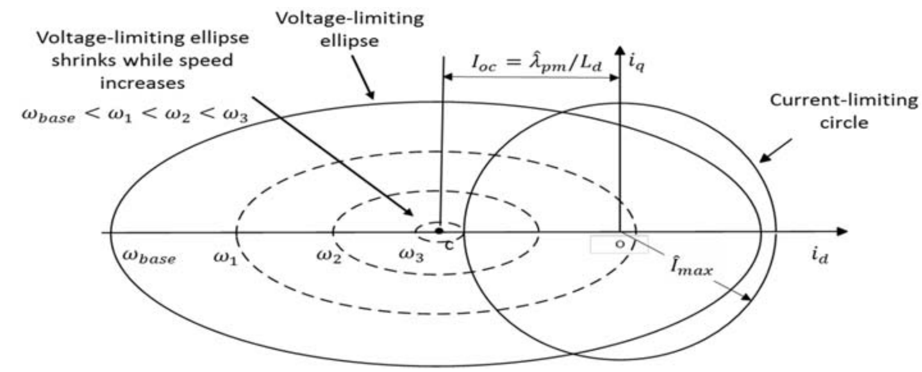

(a) Current-limiting circle and voltage-limiting ellipse for IPM motors

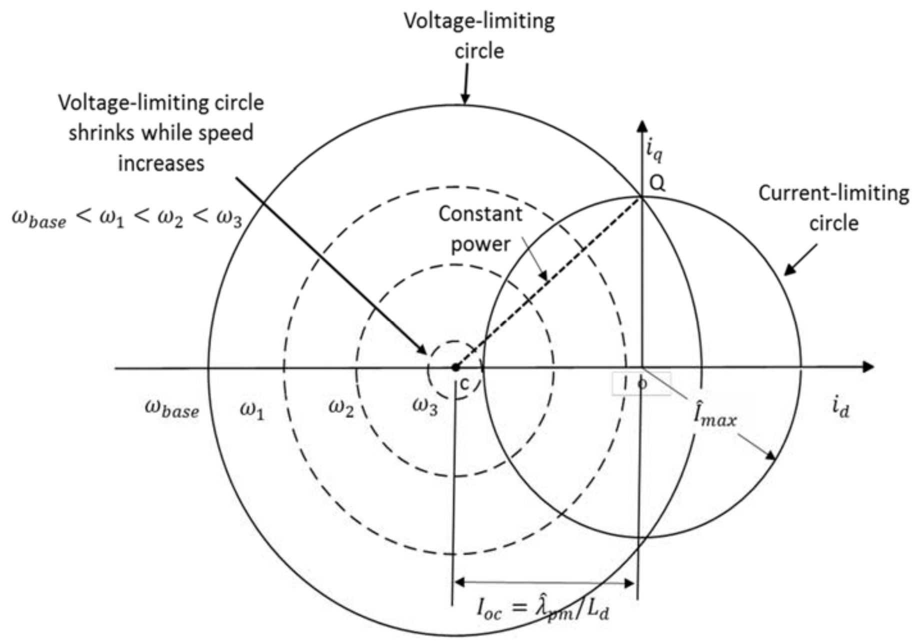

(b) Current-limiting circle and voltage-limiting circle for SPM motors

Figure 5.10: Current-limiting and voltage-limiting characteristics of PMSM.

While, the voltage limitation is an ellipse for IPM motors in the d-q frame as shown in Figure 5.10 (a), which can be derived form (5.19) as follows:

$$\frac{((\lambda_{pm} / L_d) + i_d)^2}{V_s^{\ 2} / (\omega_e L_q)^2} + \frac{i_q^{\ 2}}{V_s^{\ 2} / (\omega_e L_q)^2} = 1 \tag{5.22}$$

Where, $Vs \leq Vmax$, and $Vmax$ represents the amplitude of the maximum allowable phase voltage. However, for SPM motors, the voltage limitation becomes a circle due to the fact that $L_d = L_q$, as shown in Figure 5.10.

In the FW control category, there are several strategies used for SPM motors and IPM motors. The three commonly used FW control strategies for SPM motors are [49]:

- Constant-voltage-constant-power (CVCP) control
- Constant-current-constant-power (CCCP) control
- Voltage and current limited maximum torque (VCLMT) control

Among the three control strategies above, the VCLMT control is widely used FW control strategy for IPM motors. However, the CVCP control and CCCP control are more suitable for SPM motors.

5.3.5 Constant Voltage Constant Power (CVCP) Control for IPMSM

Among the three commonly used FW methods for SPM motors, the CVCP control is the most widely used method because of its simplicity and low requirement for additional hardware in drives. This method keeps a constant voltage and constant power by keeping the current vector following the constant power trajectory which is the dashed line in Figures 5.10 (b).

As a constant power operation, the rated power is defined as the output power, P_b, at base speed, ω_{base}, as shown in Figure 5.9. Thus, one can obtain the following:

$$P_b = \frac{\omega_{base}}{(p/2)} T_{\max} \quad \textbf{(5.23)}$$

Where, $T_{\max}$ is the maximum torque for the MTPA operation. Since the output power is constant, the output power, P_b, can be rewritten as follows:

$$P = \frac{\omega_e}{(p/2)} T_e = \text{constant} \quad \textbf{(5.24)}$$

From equation 5.23 and equation 5.24, one can obtain the following:

$$\omega_e T_e = \omega_{base} T_{\max} = \text{constant} \quad \textbf{(5.25)}$$

For SPM motors, the torque expression as previously obtained is, T_e = 3p/4 ($\lambda pm\ iq$). As aforementioned in the MTPA control section, the maximum torque for SPM motors can be obtained by keeping i_q = I_s. Thus, the maximum torque, T_{max}, can be represented as follows:

$$T_{\max} = \frac{3}{2}\frac{p}{2}\lambda_{pm} I_s \quad \textbf{(5.26)}$$

Substituting the torque expression and equation 5.26 into equation 5.25 and rearranging, one can obtain the following:

$$\omega_e i_q = \omega_{base} I_s = \text{constant} \quad \textbf{(5.27)}$$

From equation 5.27, the d-axis voltage equation can be rewritten as follows:

$$v_d = -\omega_e L_q i_q = -L_q(\omega_{base} I_s) = \text{constant} \quad \textbf{(5.28)}$$

Since the d-axis voltage is a constant value, in order to keep a constant phase voltage, the q-axis voltage has to be constant too. Moreover, since the d-axis voltage component keeps its value at the base speed, the q-axis voltage component should keep its value at the same base speed as well, which can be represented as follows:

$$v_q = v_{qb} = \text{constant} \quad \textbf{(5.29)}$$

where, v_{qb} is the q-axis voltage component at the base speed. Due to the zero d-axis current in MTPA operation for SPM motors, vqb can be written as follows:

$$v_{qb} = \omega_{base} \lambda_{pm} \quad \textbf{(5.30)}$$

Substituting $v_q = \omega_e$ (λ_{pm} + L_d i_d), and equation 5.30 into equation 5.29, one can obtain the following:

$$\omega_e(\lambda_{pm} + L_d i_d) = \omega_{base}\lambda_{pm} = \text{constant} \tag{5.31}$$

From equation 5.27 and equation 5.31, the d, q current components for the CVCP control can be obtained as follows:

$$i_d = \frac{\omega_{base}}{\omega_e}\frac{\lambda_{pm}}{L_d} - \frac{\lambda_{pm}}{L_d} \tag{5.32}$$

$$i_q = \frac{\omega_{base}}{\omega_e} I_s \tag{5.33}$$

It is obvious that the d, q current components are linearly related to each other. This relationship can be expressed as follows:

$$i_q = I_s \frac{L_d}{\lambda_{pm}} i_d + I_s \tag{5.34}$$

From equation 5.34, the CVCP trajectory can be drown as depicted in Figure 5.10, which is the line constant power line as shown in Figure 5.10 (b).

It should be noticed that the intersection point, M, between the line QC and the current-limiting circle, represents the boundary of the CVCP control. Any operation along line section MC violates the current limitation. Thus, the valid CVCP control trajectory is within the line QM in Figure 5.11.

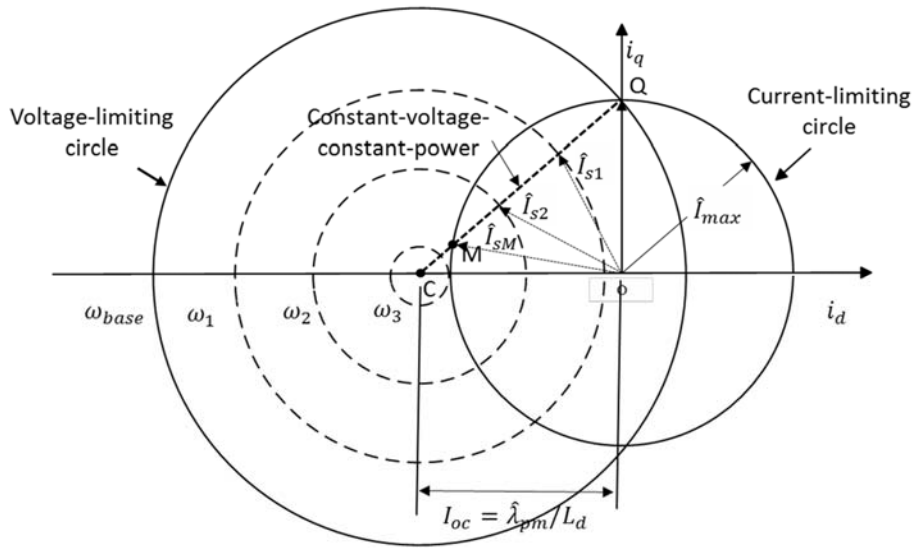

Figure 5.11: Constant-voltage-constant power control of SPM motors.

5.3.6 Constant-current-constant-power (CCCP) control for SPM motors

The CCCP control keeps a constant current and constant power by changing the q-axis voltage component. The control principle of the CCCP control is similar to the CVCP control. However, this method normally requires voltage boost capability of drives to achieve a desired voltage. Thus, it has very limited utilization.

Since the CCCP control has a constant output power as the CVCP control, the CCCP control also has a constant d-axis voltage as was previously derived in equation 5.28, which can be restated as follows:

$$v_d = -\omega_e L_q i_q = -L_q(\omega_{base} I_s) = \text{constant} \tag{5.35}$$

Thus, the q-axis current can be expressed as in equation 5.33, which yields the following:

$$i_q = \frac{\omega_{base}}{\omega_e} I_s \tag{5.36}$$

Since the CCCP control keeps a constant phase current value, by using equation 5.36 one can find the d-axis current as follows:

$$i_d = -\sqrt{{I_s}^2 - {i_q}^2} = -\frac{I_s}{\omega_e}\sqrt{{\omega_e}^2 - {\omega_{base}}^2} \tag{5.37}$$

Substituting equation 5.37 into the q-axis voltage equation, one can obtain the following:

$$v_q = \omega_e(\lambda_{pm} + L_d i_d) = \omega_e \lambda_{pm} - L_d I_s \sqrt{{\omega_e}^2 - {\omega_{base}}^2} \tag{5.38}$$

As the speed, ω_e, keeps increasing, the q-axis voltage value, v_q, experiences a slight drop and then it keeps increasing as shown in Figure 5.12. Since the d-axis voltage is constant, the phase voltage value in the CCCP control depends on the q-axis voltage component. As shown in Figure 5.13, the current trajectory of the CCCP control follows its current-limiting circle. While, the voltage trajectory changes according to the q-axis voltage.

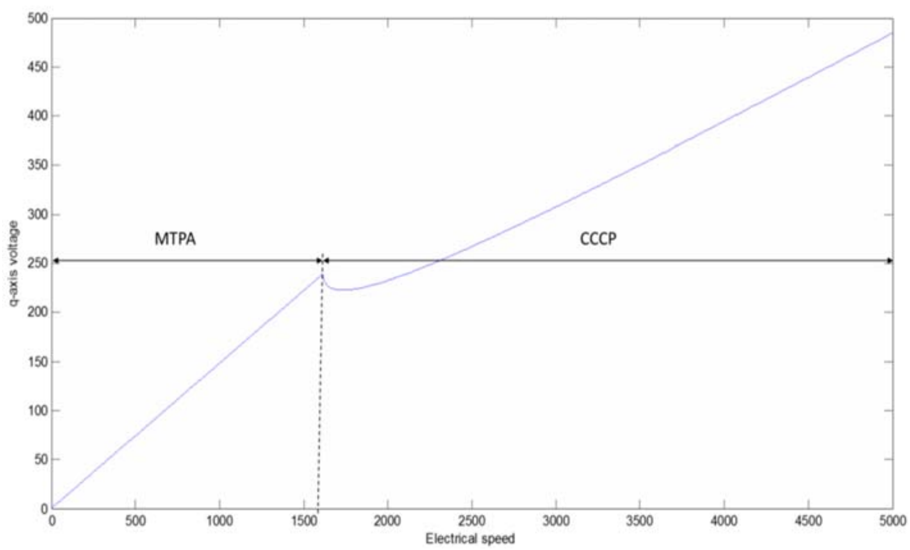

Figure 5.12: The q-axis voltage trajectory of the CCCP control.

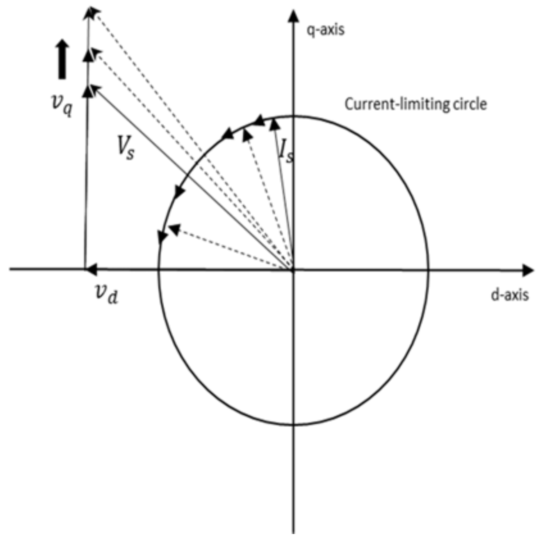

Figure 5.13: Constant-current-constant power control of SPM motors.

5.3.7 Voltage & Current Limited Maximum Torque (VCLMT) Control For IPM Motors

The VCLMT control can be employed for both SPM and IPM motors with the same operation principle. There is only a slight difference in calculations of d, q current components between the two types of PM motors. For simplicity, this section only gives the analysis of the VCLMT control for IPM motors.

As one flux weakening strategy for IPM motors, VCLMT control follows two constraints which are the current-limiting circle and the voltage-limiting ellipse, as shown in Figure 5.10 (a). As the speed increases, with the center of the ellipse remaining the same, the voltage-limiting ellipse becomes smaller and smaller as shown in Figure 5.10 (a). The i_{dm} and i_{qm} for MTPA control cannot satisfy the voltage constraint above the base speed. Therefore, new d, q current components are required to keep the maximum phase voltage, V_{max}, in the FW region. Such d, q current components can be obtained from the voltage constraint equation 5.22 as follows:

$$(L_q i_q)^2 + (L_d i_d + \lambda_{pm})^2 = \frac{V_{\max}{}^2}{\omega_e{}^2} \tag{5.39}$$

From the current-limiting circle, Figure 5.10, and equation 5.21, one can obtain the following:

$$i_q = \sqrt{I_{\max}^2 - i_d^2} \tag{5.40}$$

By substituting equation 5.40 into equation 5.39 and rearranging, a binominal equation of the d-axis current can be written as follows:

$$(L_d^2 - L_q^2)i_d^2 + 2\lambda_{pm}L_d i_d + \lambda_{pm}^2 + L_q^2 I_{\max}^2 - (V_{\max}/\omega_e)^2 = 0 \tag{5.41}$$

From equation 5.41, two solution can be obtained as follows:

$$i_{d1} = \frac{-\lambda_{pm}L_d + \sqrt{(\lambda_{pm}L_d)^2 - (L_d^2 - L_q^2)(\lambda_{pm}^2 + L_q^2 I_{\max}^2 - (V_{\max}/\omega_e)^2)}}{(L_d^2 - L_q^2)} \tag{5.42}$$

$$i_{d2} = \frac{-\lambda_{pm}L_d - \sqrt{(\lambda_{pm}L_d)^2 - (L_d^2 - L_q^2)(\lambda_{pm}^2 + L_q^2 I_{\max}^2 - (V_{\max}/\omega_e)^2)}}{(L_d^2 - L_q^2)} \tag{5.43}$$

Since the demagnetizing current should be a negative value, the root i_{d1} in equation 5.43 is the expected useful solution for the FW operation. From the above analysis of the VCLMT strategy, the d- and q-axis currents for the FW control of IPM motors can be expressed as follows:

$$i_{d,VCL} = \frac{-\lambda_{pm}L_d - \sqrt{(\lambda_{pm}L_d)^2 - (L_d^2 - L_q^2)(\lambda_{pm}^2 + L_q^2 I_{\max}^2 - (V_{\max}/\omega_e)^2)}}{(L_d^2 - L_q^2)} \tag{5.44}$$

$$i_{q,VCL} = \sqrt{I_{\max}^2 - i_{d,VCL}^2} \tag{5.45}$$

For the whole speed range of operation, a recommended control strategy for IPM motor is the combination of the MTPA control and FW control. The optimal current vector trajectory for the MTPA control and the FW control is shown in Figure 5.14. This strategy implements the MTPA control in the low speed region, which is region OA as shown in Figure 5.14, until the base speed. Then, it employs the FW control at region AB, when the speed is above base speed.

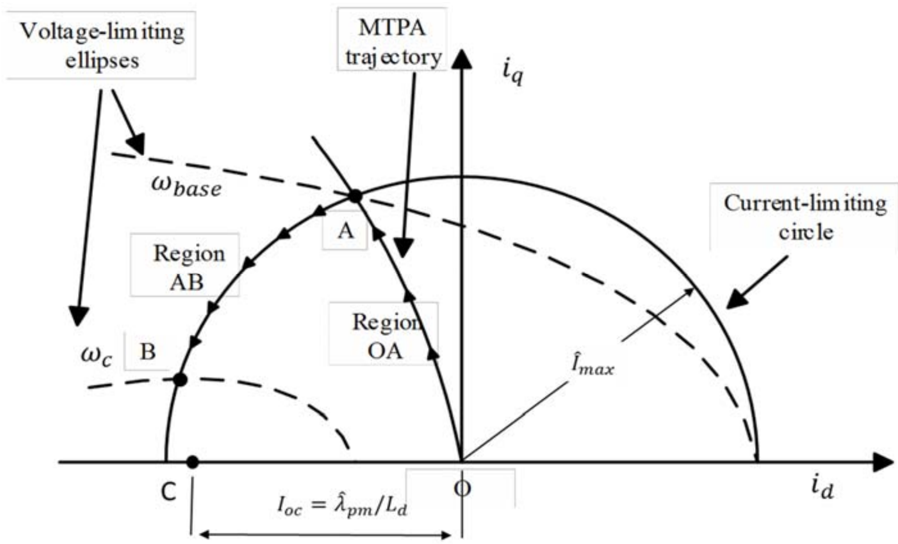

(a) $\lambda_{pm} / L_d < I_{\max}$

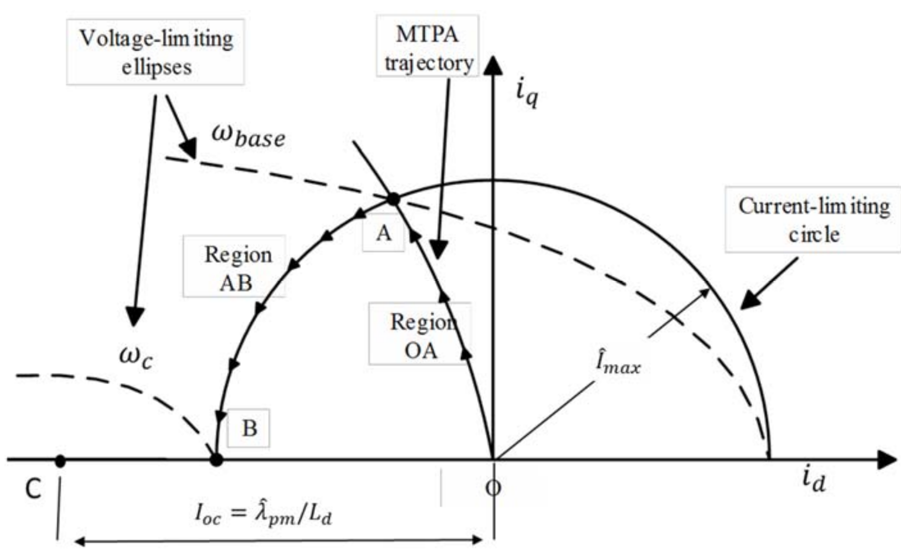

(b) $\lambda_{pm} / L_d > I_{\max}$

Figure 5.14: Optimum current vector trajectory in the d, q frame for IPM motors.

From the voltage ellipse equation 5.21, the center of the voltage ellipse is located at a point C ($-\lambda_{pm}/$, 0), as shown in Figures 5.10 and 5.14. Notice that λ_{pm}/L_d is usually defined as the short circuit current. Once the maximum inverter current, I_{max}, becomes equal to or larger than the short circuit current, the permanent magnet can be fully demagnetized. In another word, the permanent magnet flux, λ_{pm}, can be fully cancelled/eliminated.

With a large size inverter which has $I_{max} > (\lambda_{pm}/L_d)$ as shown in Figure 5.14 (a), the lossless machine is capable of attaining infinite speed. Above a certain speed at point B, the maximum torque becomes only voltage limited. Then the current trajectory follows the voltage ellipse rather than the current circle for the maximum torque.

With a small size inverter which has $I_{max} < (\lambda_{pm}/L_d)$ as shown in Figure 5.14 (b), the maximum speed at point B is finite. The maximum torque can be found at the intersection between the voltage limiting ellipse for that speed and the current-limiting circle. In most design cases, we only have $I_{max} < (\lambda_{pm}/L_d)$, which means that the permanent magnet is too strong to be fully demagnetized.

Since the more demagnetizing current in the negative d-axis direction the deeper the flux weakening, the maximum speed of the VCLMT control can be obtained by substituting $i_d = -I_{max}$ and $i_q = 0$ into (5.39) as follows:

$$(-L_d I_{\max} + \lambda_{pm})^2 = \frac{V_{\max}^{\ 2}}{\omega_e^{\ 2}} \tag{5.46}$$

or

$$\omega_e = \frac{V_{\max} / L_d}{(\lambda_{pm} / L_d - I_{\max})} \tag{5.47}$$

For a large size inverter, the denominator in equation 5.47 could be zero. Therefore, the theoretical speed is infinite.

6. SIMULATIONS

6.1 Drive System Simulations

This chapter describes different tools available for electrical and electronic systems simulation and then justification is given for selecting Simulink for the IPMSM system. Block by block an explanation is given for Simulink simulation of the drive system.

6.2 Simulation Tools

Study of electric motor drives needs the proper selection of a simulation tool. Their complex models need computing tools capable of performing dynamic simulations. Today with the growth in computational power there is a wide selection of software titles available for electrical simulations such as ACSL, ESL, EASY5, and PSCSP are for general systems and SPICE2, EMTP, and ATOSEC5 for simulating electrical and electronic circuits. IESE and SABER are examples of general-purpose electrical network simulation programs that have provisions for handling user-defined modules. SIMULINK® is a toolbox extension of the MATLAB program. It is a program for simulating dynamic systems [13].

Simulink has the advantages of being capable of complex dynamic system simulations, graphical environment with visual real time programming and broad selection of tool boxes[12]. The simulation environment of Simulink has a high flexibility and expandability which allows the possibility of development of a set of functions for a detailed analysis of the electrical drive [12]. Its graphical interface allows selection of functional blocks, their placement on a worksheet, selection of their functional parameters interactively, and description of signal flow by connecting their data lines using a mouse device. System blocks are constructed of lower level blocks grouped into a single maskable block. Simulink simulates analogue systems and discrete digital systems[16].

6.3 IPMSM Drive Components

The PM motor drive simulation was built in several steps like abc phase transformation to dqo variables, calculation torque and speed, and control circuit. The abc phase transformation to dqo variables is built using Parks transformation and for the dqo to abc the reverse transformation is used. For simulation purpose the voltages are the inputs and the current are output. Parks transformation used for converting Vabc to Vdqo is shown in Figure 6.1 and the reverse transformation for converting Idqo to Iabc is shown in Figure 6.2.

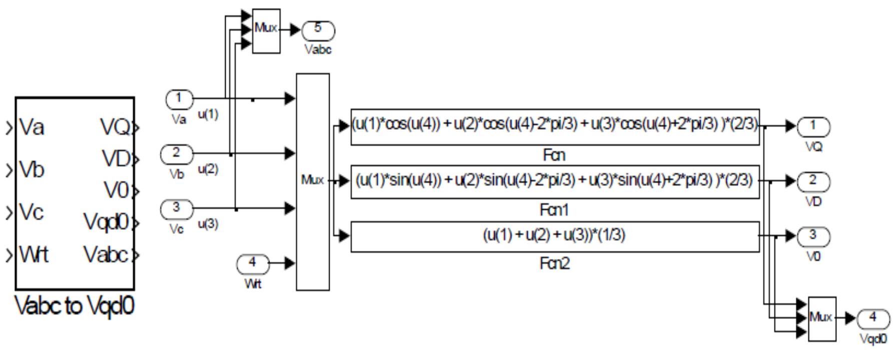

Figure 6.1: Vabc to Vdqo block.

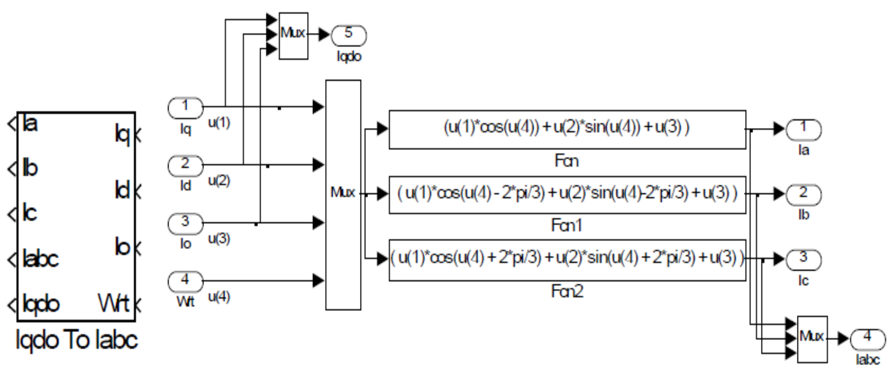

Figure 6.2: Idqo to Iabc block.

The motor equations explained before are used to establish the motor model in Simulink. Figure 6.3 shows the motor model used.

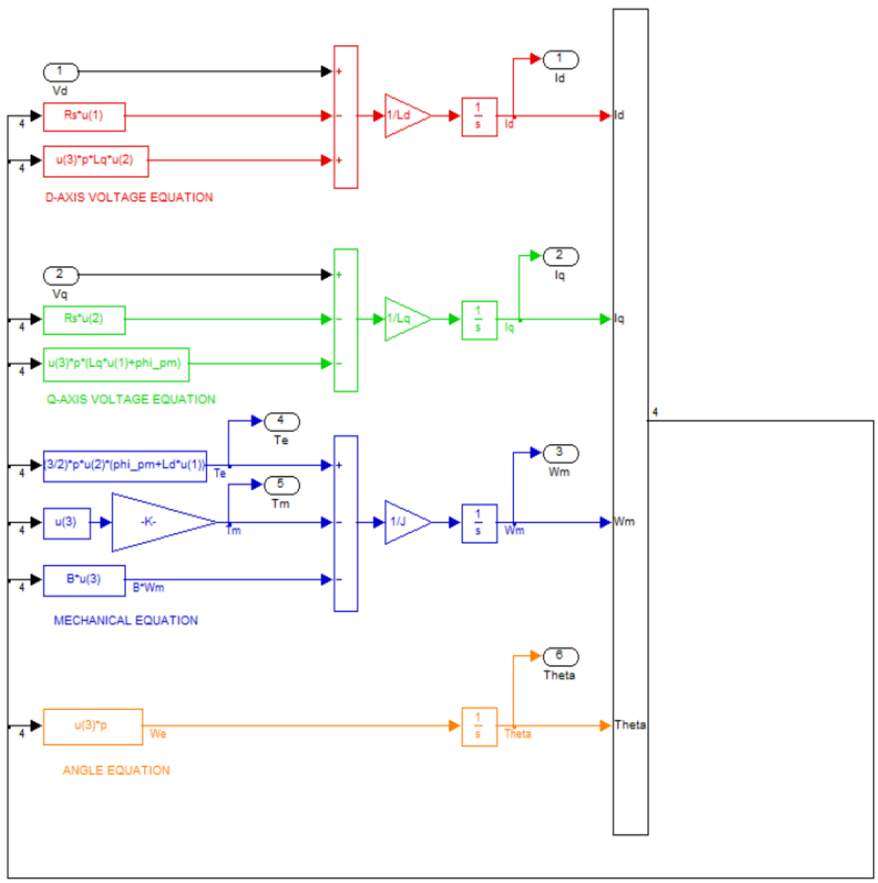

Figure 6.3: Simulink model of the IPMSM.

Figure 6.4 shows the torque block in Simulink. This block is developed by using the torque equation:

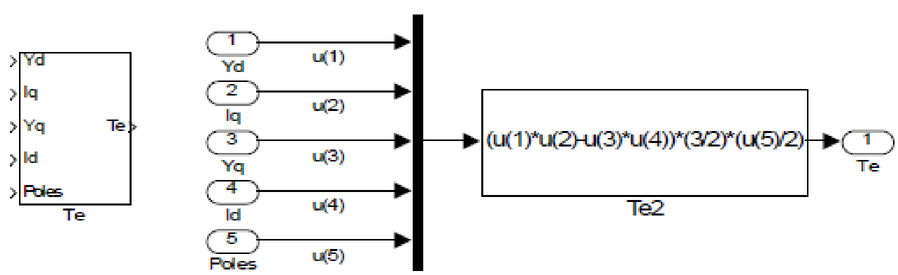

Figure 6.4: Torque Block.

The speed of the motor is obtain using Figure 6.5. The developed speed block is shown in Figure 6.5.

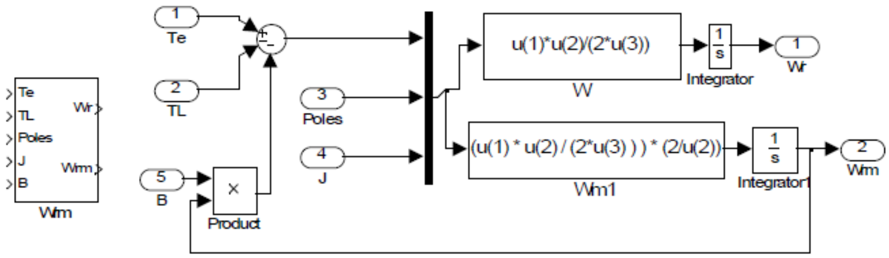

Figure 6.5: Speed Block.

The inverter is implemented in Simulink as shown in Figure 6.6. The inverter consists of the "universal bridge" block from the power systems tool box with the parameters of the IGBT that was presented in chapter 2. The voltages and currents in the motor and in all the devices of the inverter can be obtained. The losses in the inverter and motor can be calculated.

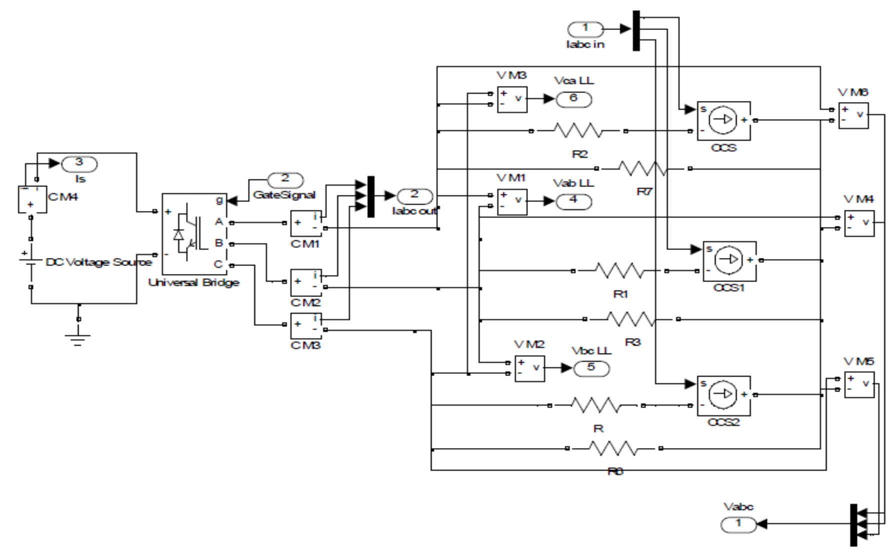

Figure 6.6: Voltage Source Inverter.

For proper control of the inverter using the reference currents, current controllers are implemented to generate the gate pulses for the IGBT's. Current controllers used are shown in Figure 6.7.

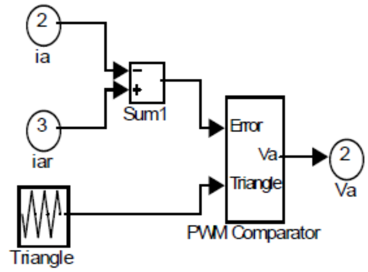

Figure 6.7: PWM Current Controller

In Figure 6.8 the whole controller system is presented. There are many control schemes published in the literatures that combines the MTPA control and the FW control [22-24]. Figure 4.6 shows the specially designed control scheme for IPMSMs driven by ZSIs, which is based on speed control schemes presented in [22-24]. The proposed control scheme in Figure 6.8 consists of three major controllers, namely, the speed regulator in Part A, the current regulator in Part B, and the BVFW regulator in Part C.

Assuming the controlled motor is in the stop or standby state, a commanded speed reference speed , is first sent into the control loop and compared to the feedback speed, which is the motor's real speed obtained from an encoder. Then the error difference between the reference speed and the real speed is sent into the speed controller in Part A. According to this speed error, a reference value of the amplitude of the phase currents, is generated by the speed regulator. Notice that in this speed control scheme, there is no reference torque. In order to obtain the maximum torque during the full speed range, the reference phase current during the MTPA control and the FW control is set to its maximum value. Such phase current will be send into the MTPA block which yields the reference d-axis current component, for the MTPA control. It has to be emphasized that the FW regulator has zero output before the speed reaches the base speed. Therefore, during the constant torque region, the reference demagnetizing current for the FW control is zero. Then the reference q-axis current can be obtained from current equation. In the constant power region, where the speed is above the base value, all the components in Part A are still active. However, the BVFW regulator in Part C starts to yield an extra demagnetizing current. With the reference DQ axis current components, the two reference voltage components can be obtained from the current regulator in Part B.

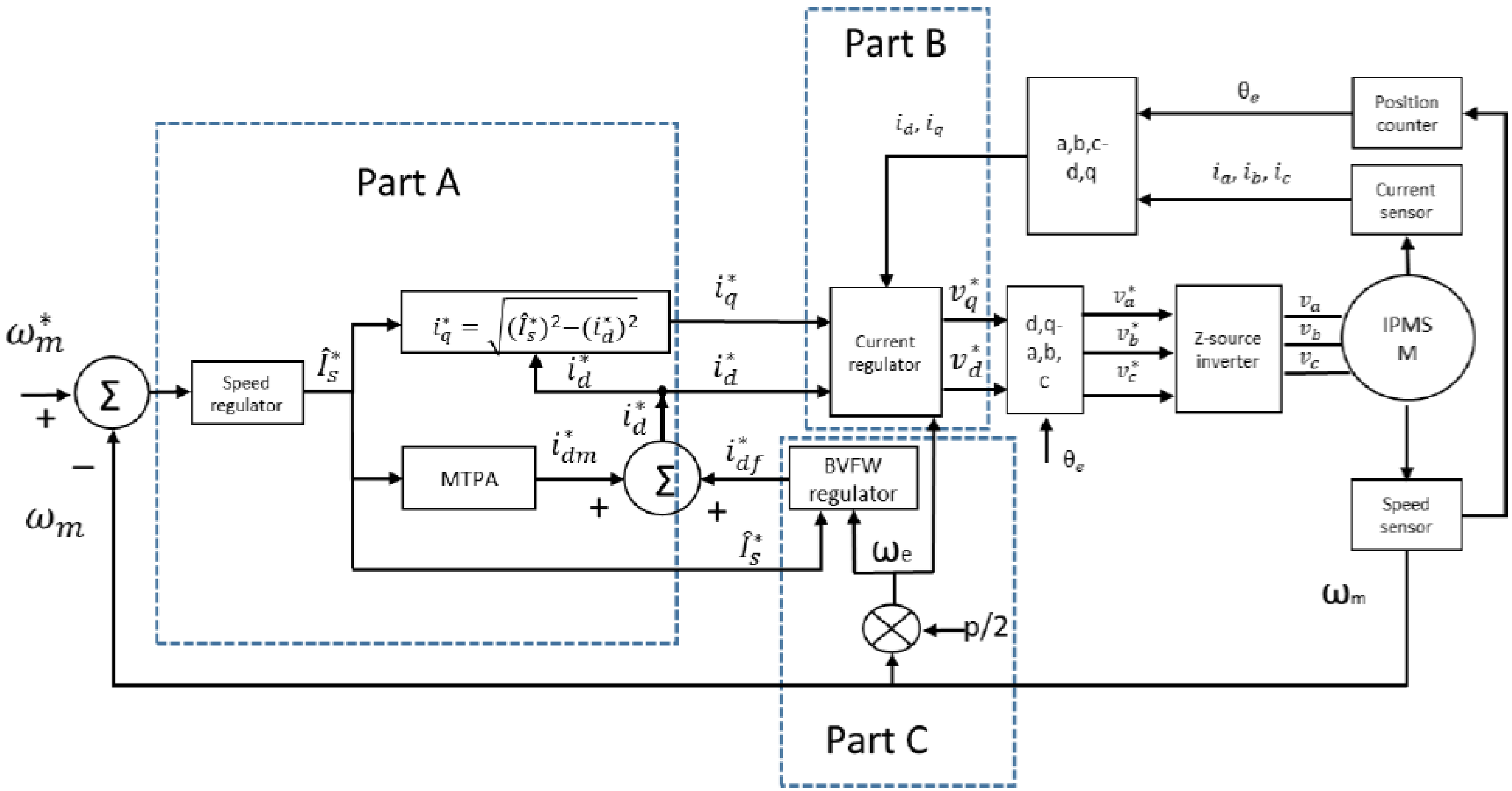

Figure 6.8: Control diagram for IPMSM.

6.4 Design Procedure of the PI Controller

The PI controller shown in Figure 6.8 is responsible for generating the necessary voltage for achieving ommanded speed and must be designed carefully for satisfactory performance. In this section, the steps taken for analyzing the system and going through a successful design procedure for the PI controller will be described.

Any mechanical rotating body with inertia J and damping coefficient B_c can be expressed using the following differential equation under a load torque of T_L [46][47]

$$T_e = J\frac{d\omega}{dt} + B_c\omega + T_L \tag{6.1}$$

To get a linear transfer function, the load torque can be considered as an increase in damping coefficient and thus equation 6.1 can be rewritten as:

$$T_e = J\frac{d\omega}{dt} + B_c\omega \tag{6.2}$$

This gives the following linear transfer function in the Laplace domain:

$$\omega(s) = \frac{T_e(s)}{Js + B_c} \tag{6.3}$$

Instead of using the mechanical speed as a measure of speed, electrical speed in radians per second was considered to avoid conflict with the electrical speed used in all voltage current relationships. At this point, a relationship between voltage magnitude v_m and produced torque T_e must be determined.

$$T_e = (k_1 + k_2(\frac{1}{Z_m{}^2}(RV\cos\delta - \omega R\phi_m + \omega L_d V\sin\delta)))$$
$$(\frac{1}{Z_m{}^2}(-RV\sin\delta) - \omega^2 L_q\phi_m + \omega L_q V\cos\delta)) \tag{6.4}$$

where $Z_m{}^2 = R^2 + \omega^2 L_d L_q$, $k_1 = \frac{3}{2}\frac{p}{2}\phi_m$, $k_2 = \frac{3}{2}\frac{p}{2}(L_d - L_q)$

Equation 6.4 provides a straight forward relationship between torque output and applied voltage at a certain speed. Algebraic manipulation on equation 6.4 provides the following torque equation:

$$T_e = F_1(\omega,\delta) + F_2(\omega,\delta)V + F_3(\omega,\delta)V^2 \tag{6.5}$$

where,

$$F_1(\omega,\delta) = \frac{k_1}{Z_m{}^2}\omega R_s\phi_m + \frac{k_2}{Z_m{}^4}\omega^3 L_q R_s\phi_m{}^2 \tag{6.6}$$

$$F_2(\omega,\delta) = -\frac{k_1}{Z_m{}^2}R_s\cos\delta + \frac{k_1}{Z_m{}^2}\omega L_d\sin\delta + \frac{k_2}{Z_m{}^4}R_s{}^2\omega\phi_m\sin\delta$$
$$-\frac{k_2}{Z_m{}^4}R_s\omega^2\phi_m L_q\cos\delta - \frac{k_2}{Z_m{}^4}\omega^3\phi_m L_d L_q\sin\delta \tag{6.7}$$

$$F_3(\omega,\delta) = -\frac{k_2}{Z_m{}^4}R_s{}^2\sin\delta\cos\delta + \frac{k_2}{Z_m{}^4}R_s\omega L_d\sin^2\delta$$
$$+\frac{k_2}{Z_m{}^4}\omega L_q R_s\cos^2\delta + \frac{k_2}{Z_m{}^4}\omega^2 L_d L_q\sin\delta\cos\delta \tag{6.8}$$

Using equation 6.5 in equation 6.2 gives the following differential equation in the time domain:

$$\dot{\omega} = -B_c\omega + F_1(\omega,\delta) + F_2(\omega,\delta)V + F_3(\omega,\delta)V^2 \tag{6.9}$$

here, $\dot{\omega}, \omega, \delta$ are all time varying quantities. Equation 6.9 is clearly a non-linear function of voltage reference and thus difficult to analyze for PI controller design. A linearization of the non-linear function around a nominal operating point would be helpful in the design process [48]. If ω_n and V_n are the nominal system input and output respectively, then equation 6.9 can be rewritten as:

$$\dot{\omega}_n + \Delta\dot{\omega} = -B_c\omega_n - B_c\Delta\omega + F_1(\omega,\delta) + F_2(\omega,\delta)V + F_3(\omega,\delta)V^2 \tag{6.10}$$

δ is assumed constant in the modeling as the bandwidth of the PI controller is much faster than the variation in δ. The right hand side of the expansion can be expressed using a Taylor series expansion ignoring the higher order terms. Thus

$$\begin{aligned}\dot{\omega}_n + \Delta\dot{\omega} &= -B_c\Delta\omega + \frac{\partial F_1(\omega_n)}{\partial\omega}\Delta\omega + \frac{\partial F_2(\omega_n)V_n}{\partial\omega}\Delta\omega + \frac{\partial F_3(\omega_n)V_n^{\;2}}{\partial\omega}\Delta\omega \\ &+ \frac{\partial F_1(\omega_n)}{\partial\omega}\Delta V + \frac{\partial F_2(\omega_n)V_n}{\partial\omega}\Delta V + \frac{\partial F_3(\omega_n)V_n^{\;2}}{\partial\omega}\Delta V\end{aligned} \tag{6.11}$$

The derivatives of $F_1(\omega)$, $F_2(\omega)$ and $F_3(\omega)$ with respect to ω around the nominal speed of ω_n were found numerically since the functions containing ω are highly non-linear. Derivatives with respect to the voltage were quite simple to compute since $F_1(\omega)$, $F_2(\omega)$ and $F_3(\omega)$ are independent of V. Performing all the computations, equation 6.11 can be rewritten as:

$$\Delta\dot{\omega} = G\Delta\omega + H\Delta V \tag{6.12}$$

where,

$$G = -B_c + \frac{\partial F_1(\omega_n)}{\partial\omega} + \frac{\partial F_2(\omega_n)V_n}{\partial\omega} + \frac{\partial F_3(\omega_n)V_n^{\;2}}{\partial\omega} \tag{6.13}$$

$$H = F_2(\omega_n) + 2V_nF_3(\omega_n) \tag{6.14}$$

Taking the Laplace transformation, the following transfer function results

$$\Delta\omega(s) = \frac{H\Delta V(s)}{s-G} \quad \textbf{(6.15)}$$

Considering the operating voltage range of the experimental and simulation model of the IPM, 25 V was chosen as a nominal voltage. Using the steady state parameters of the IPM, the nominal speed is found to be 143.8 rad/sec for 25 V operation with 0.015 Nm*sec/rad damping coefficient. Thus, considering ω_n=143.8 rad/sec, V_n=25 V and B_c=0.015 Nmsec/rad, the following linearized transfer function was obtained:

$$\Delta\omega(s) = \frac{167.8 \cdot \Delta V(s)}{s+47.68} \quad \textbf{(6.16)}$$

Figure 6.9 shows the frequency response of the linearized system. Since the PI controller is responsible for maintaining reference speed, a system with slower response time is required. Thus, a PI controller should be chosen to increase the DC gain to achieve lower steady state error, at the same time maintaining smaller gain at higher frequencies.

Figure 6.10 shows the frequency response of the PI controller with Kp=0.1671 and Ki=0.9549. Transfer function of the PI controller is thus given by

$$\Delta V(s) = \frac{0.1671 \cdot s + 0.9549}{s} \Delta\omega_{error} \quad \textbf{(6.17)}$$

Frequency response of the combined system is shown in Figure 6.11. The system has a crossover frequency of 4 rad/sec, which is sufficient for the speed control loop.

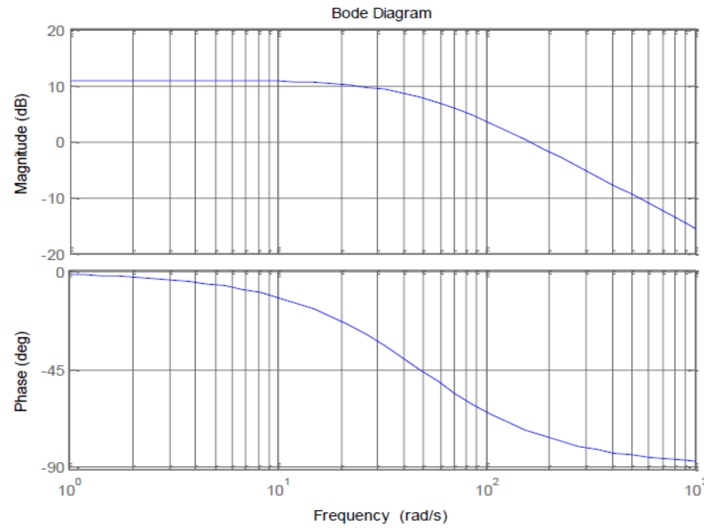

Figure 6.9: Frequency response of the linearized system at ωn = 143.8 rad/sec.

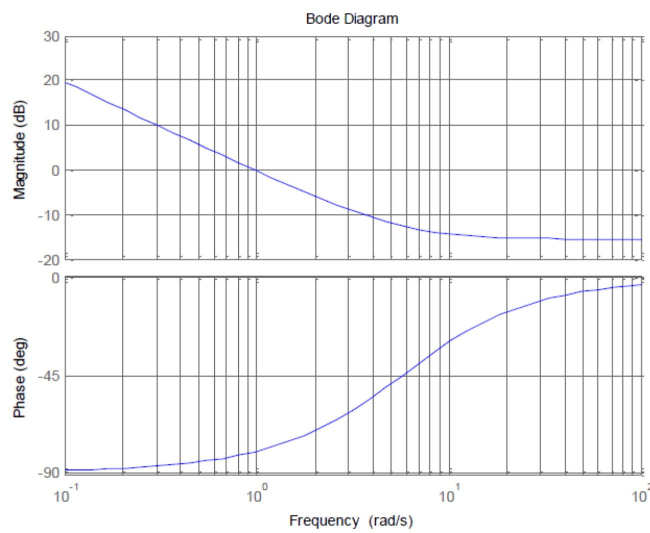

Figure 6.10: Frequency response of the PI controller.

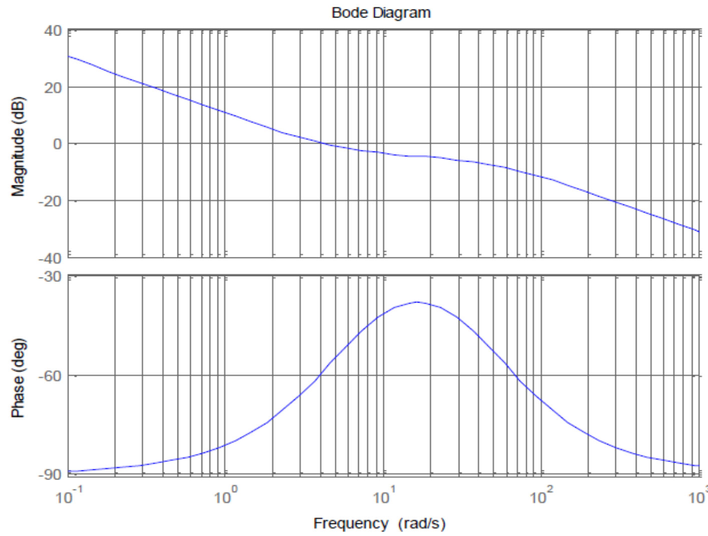

Figure 6.11: Frequency response of the combined system.

7. RESULTS

7.1 Simulation Results

In this chapter, the effectiveness of the proposed algorithm is verified at both transient and steady state conditions through simulations. Performance of the control scheme at different regions is discussed as well.

All of the simulations were done with a DC link voltage of 325 V_{DC} an 20 μs sample time. The simulations consist of two phases; an acceleration part and a constant speed part. During the accelerating part, the motor delivers full torque until it reaches its reference speed, the torque then drops to the same value as the load to keep the speed constant.

7.1.1 Test 1: Load = 100 Nm && Speed = 3000 rpm

In the first simulation, the load torque was set to 100 Nm. Under this load, the motor speeded upto 3000 rpm. These conditions helped us analyze the controler's performance for constant torque and flux weakening regions. As it can be seen from the below figures the perofrmance of the controller was very good, even when the motor kept speeding up from the base speed to higher speeds.

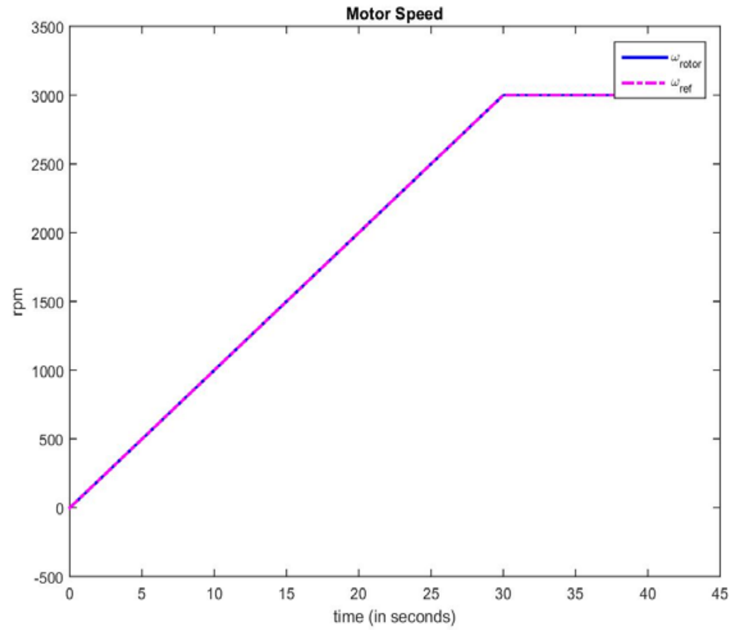

Figure 7.1: Test 1 ~ Speed analysis of the motor

Under the load of 100 Nm, the motor was asked to speed up to 3000 rpm and the resulting speed, torque and currents were analyzed. It can be seen from the Figure 7.1 that the speed controler was doing a very good job.

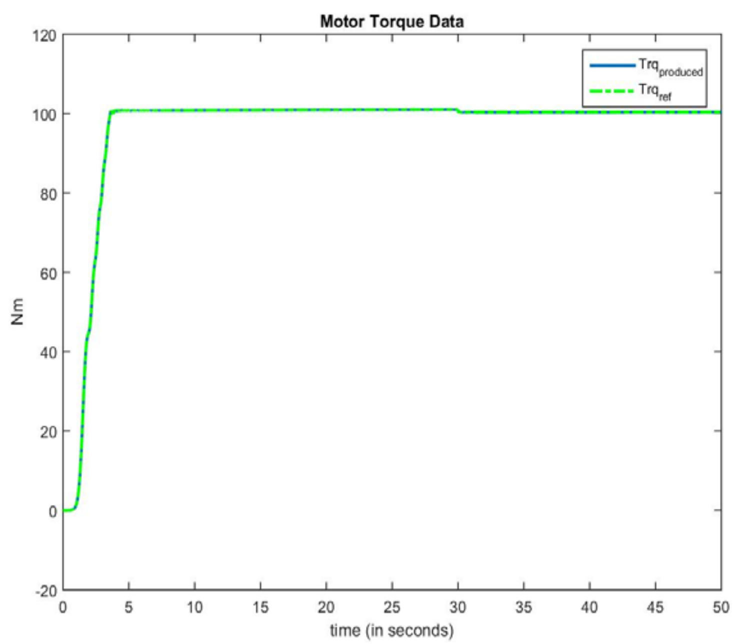

Figure 7.2: Test 1 ~ Torque analysis of the motor.

The explained cascaded controller's performance was also analyzed in respect to torque outcome. From Figure 7.2 we can clearly seeing that the control algorithm for constant torque region which is chosen as MTPA control, easily achieved the required torque for given speed.

Figures 7.3 to 7.5 are showing the current generated under the given test conditions. With the proposed control algorithm, we were able to reach the given torque and speed demands within the predefined current and voltage limits.

When we look at the reference DQ axis current components shown in Figures 7.3 and 7.4, the current trajectories are consistent with their reference values. It is obvious that the demagnetizing current, id, is increasing in the negative direction during the FW region. Meanwhile the q-axis current, iq is decreasing.

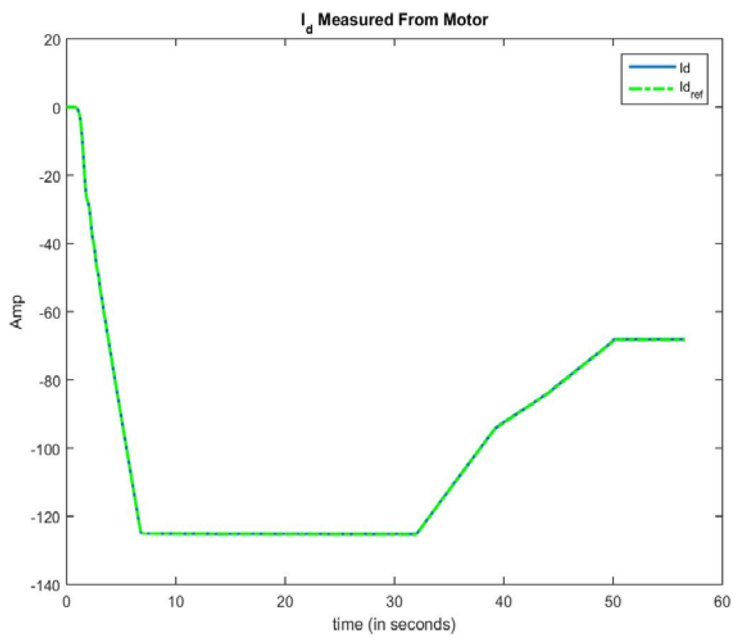

Figure 7.3: Test 1 ~ D axis current (ref vs sim).

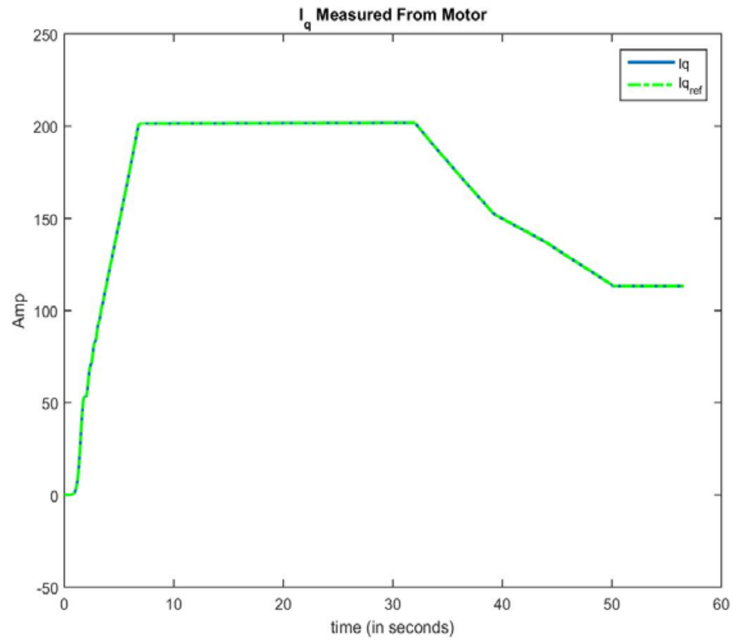

Figure 7.4: Test 1 ~ Q axis current (ref vs sim).

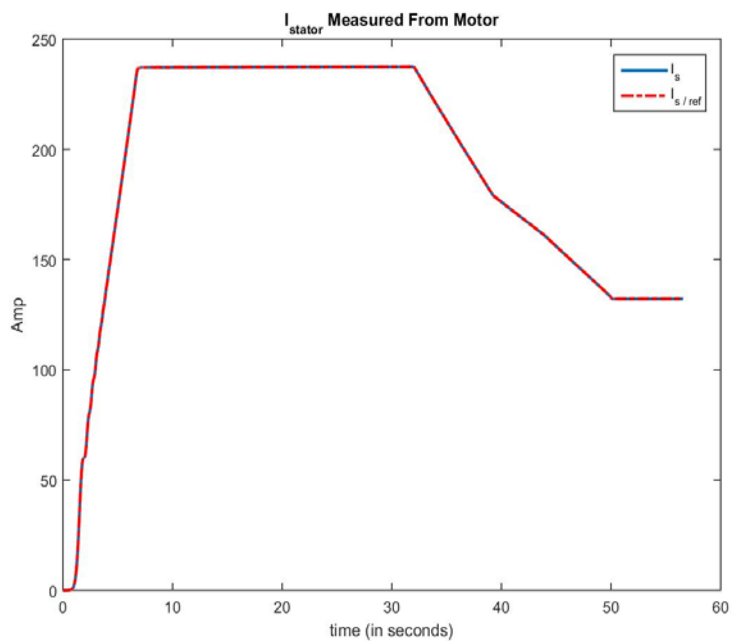

Figure 7.5: Test 1 ~ Stator current (ref vs sim).

Also in Figure 7.6 and 7.7, the power and energy demands were analyzed for the given test requirements. Including the imperfections, we can see the losses in energy conversions due to inverter, battery and motor efficiency criteria.

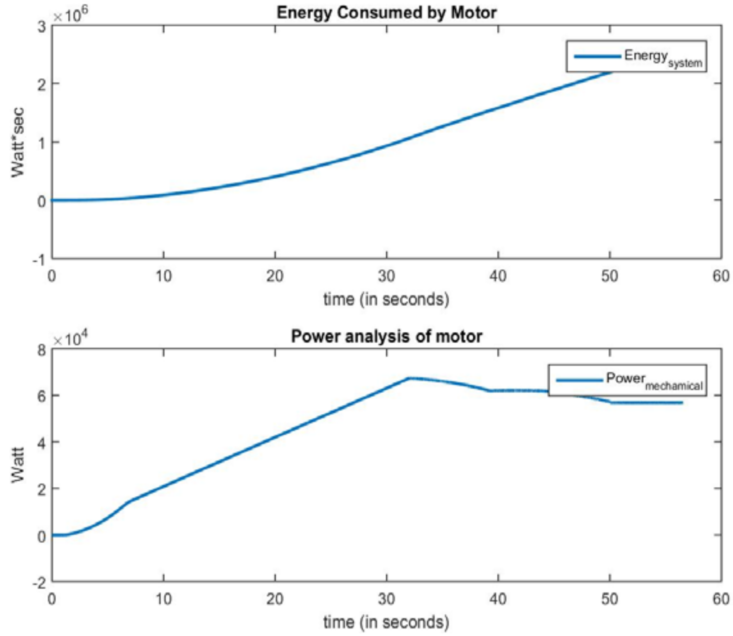

Figure 7.6: Test 1 ~ Power analysis of the motor.

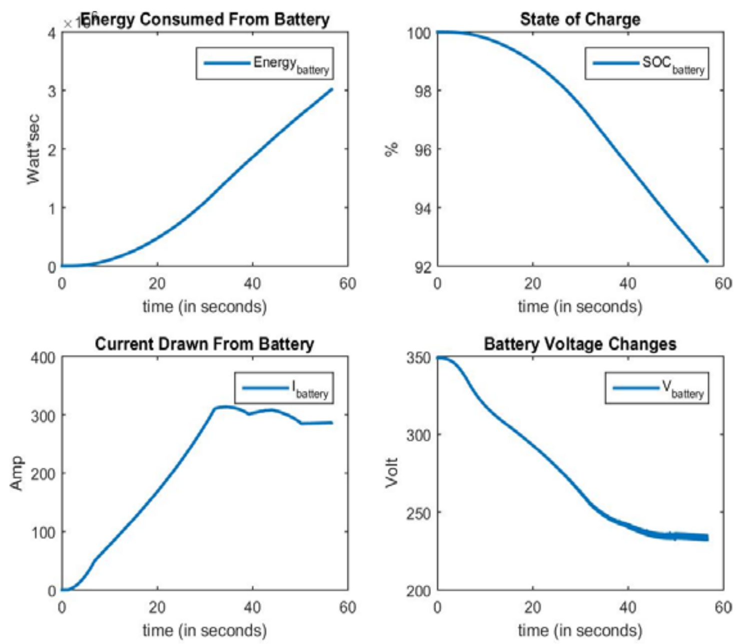

Figure 7.7: Test 1 ~ Power analysis of the battery.

From the simulation results presented here, the implemented control system shows reliable performances during the low speed constant torque region and during the high-speed constant power region. The error between the motor's final speed and the reference speed is small. Despite some torque ripples, the developed torque remains at a constant value at low speed with the MTPA control. While, the output power is roughly remaining at a constant value during FW region with the flux weakening control. From these simulation results, one can arrive at a conclusion that this flux weakening control algorithm is a valid flux-weakening control method.

7.1.2 Test 2: Load = 200 Nm && Speed = 2000 rpm

In the second simulation, the load torque was set to 200 Nm. Under this load, the motor speeded upto 2000 rpm. These conditions helped us analyze the controler's performance for constant torque region. As it can be seen from the below figures the perofrmance of the controller was very good.

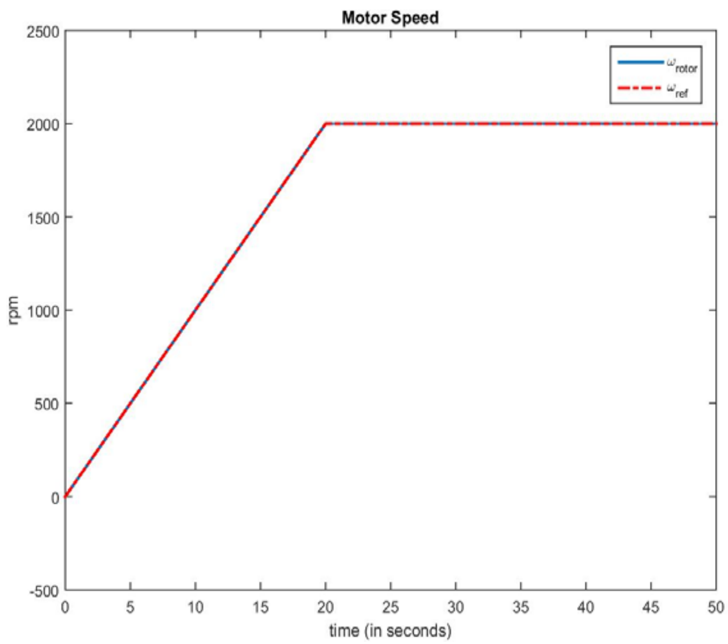

Figure 7.8: Test 2 ~ Speed analysis of the motor

Under the load of 200 Nm, the motor was asked to speed up to 2000 rpm and the resulting speed, torque and currents were analyzed. It can be seen from the Figure 7.8 that the speed controler was doing a very good job.

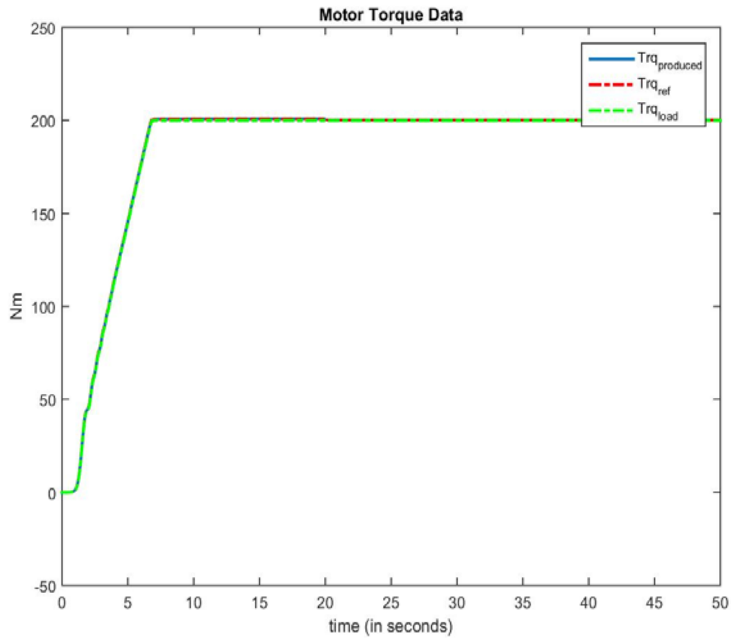

Figure 7.9: Test 2 ~ Torque analysis of the motor.

The explained cascaded controller's performance was also analyzed in respect to torque outcome. From Figure 7.9 we can clearly seeing that the control algorithm for constant torque region which is chosen as MTPA control, easily achieved the required torque for given speed.

Figures 7.10 to 7.12 are showing the current generated under the given test conditions. With the proposed control algorithm, we were able to reach the given torque and speed demands within the predefined current and voltage limits.

When we look at the reference DQ axis current components shown in Figures 7.10 and 7.11, the current trajectories are consistent with their reference values. It is obvious that the demagnetizing current, id, is increasing in the negative direction during the FW region. Meanwhile the q-axis current, iq is decreasing.

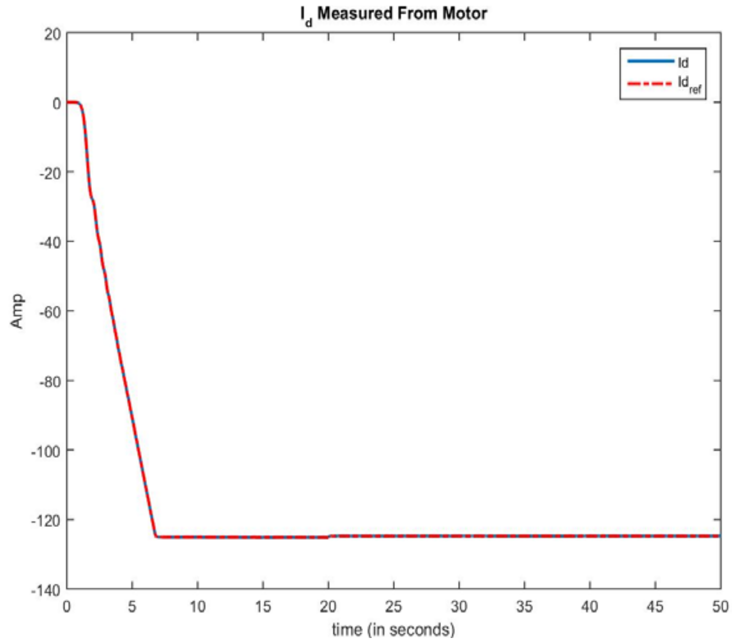

Figure 7.10: Test 2 ~ D axis current (ref vs sim).

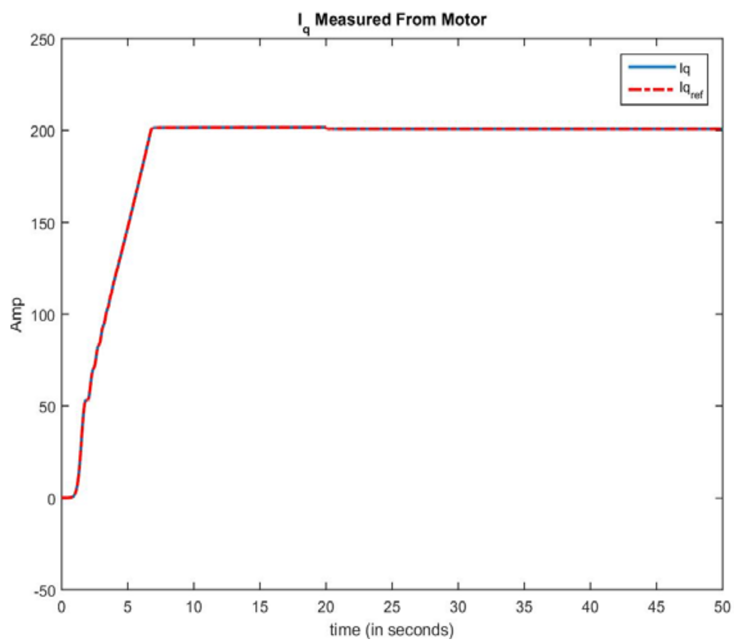

Figure 7.11: Test 2 ~ Q axis current (ref vs sim).

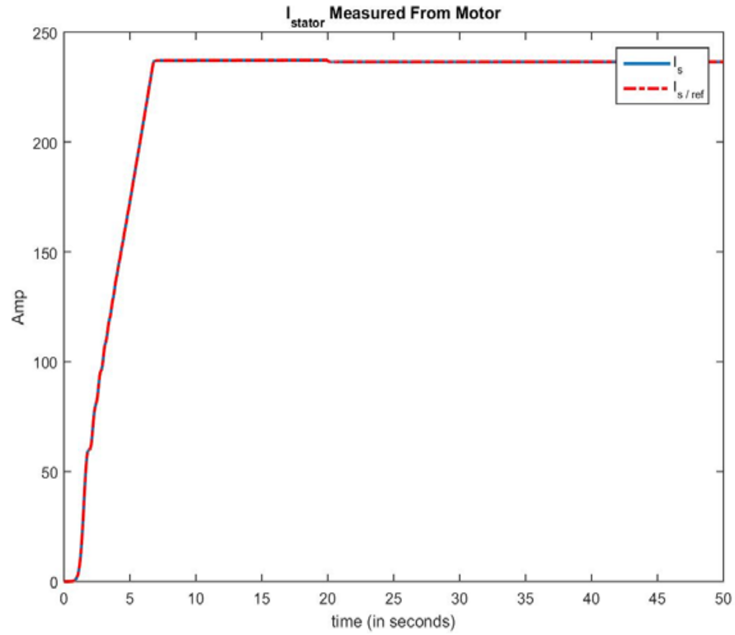

Figure 7.12: Test 2 ~ Stator current (ref vs sim).

From the simulation results presented here, the implemented control system shows reliable performances during the low speed constant torque region and during the high-speed constant power region. The error between the motor's final speed and the reference speed is small. Despite some torque ripples, the developed torque remains at a constant value at low speed with the MTPA control. While, the output power is roughly remaining at a constant value during FW region with the flux weakening control. From these simulation results, one can arrive at a conclusion that this flux weakening control algorithm is a valid flux-weakening control method.

7.1.3 Test 3: Load = 200 Nm && Speed = 5000 rpm

In the third simulation, the load torque was set to 200 Nm. Under this load, the motor speeded upto 5000 rpm. These conditions helped us analyze the controler's performance for high speed region. As it can be seen from the below figures the perofrmance of the controller was very good, even when the motor past its critical speed.

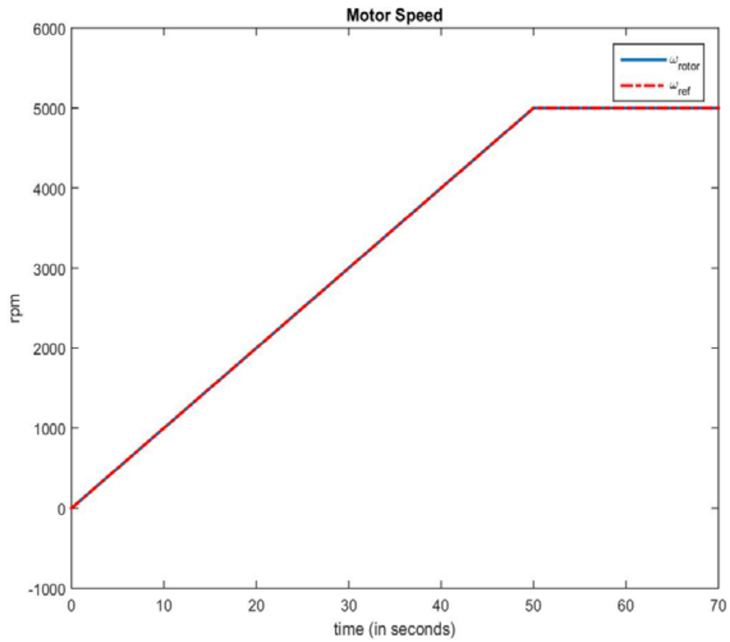

Figure 7.13: Test 3 ~ Speed analysis of the motor

Under the load of 200 Nm, the motor was asked to speed up to 5000 rpm and the resulting speed, torque and currents were analyzed. It can be seen from the Figure 7.13 that the speed controler was doing a very good job.

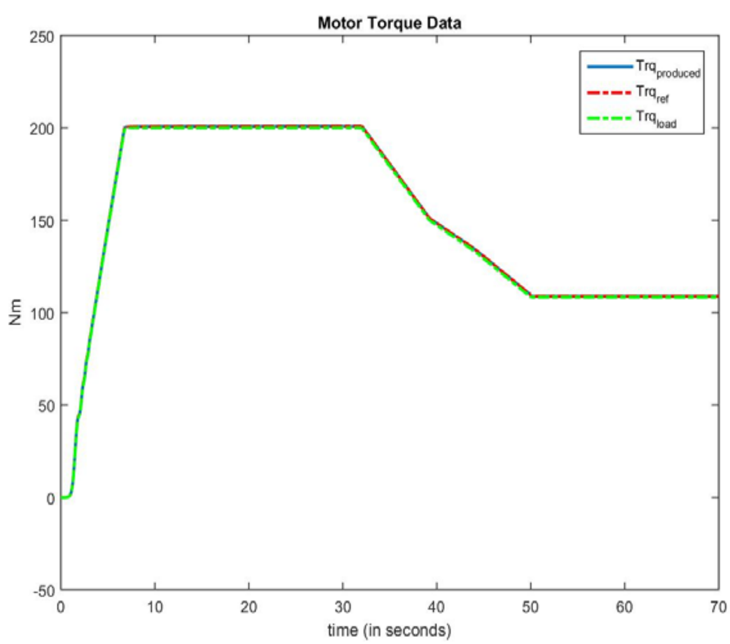

Figure 7.14: Test 3 ~ Torque analysis of the motor.

The explained cascaded controller's performance was also analyzed in respect to torque outcome. From Figure 7.14 we can clearly seeing that the control algorithm for constant torque region which is chosen as MTPA control, easily achieved the required torque for given speed.

Figures 7.15 to 7.17 are showing the current generated under the given test conditions. With the proposed control algorithm, we were able to reach the given torque and speed demands within the predefined current and voltage limits.

When we look at the reference DQ axis current components shown in Figures 7.15 and 7.16, the current trajectories are consistent with their reference values. It is obvious that the demagnetizing current, id, is increasing in the negative direction during the FW region. Meanwhile the q-axis current, iq is decreasing.

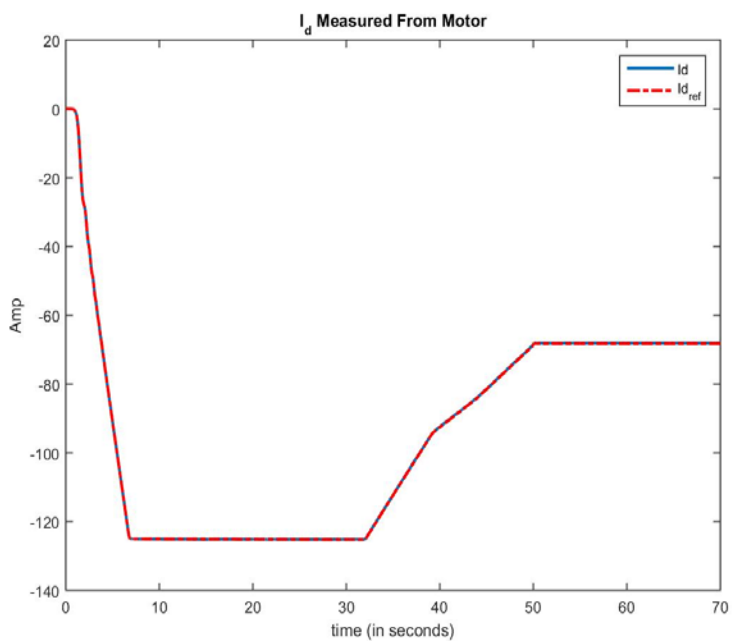

Figure 7.15: Test 3 ~ D axis current (ref vs sim).

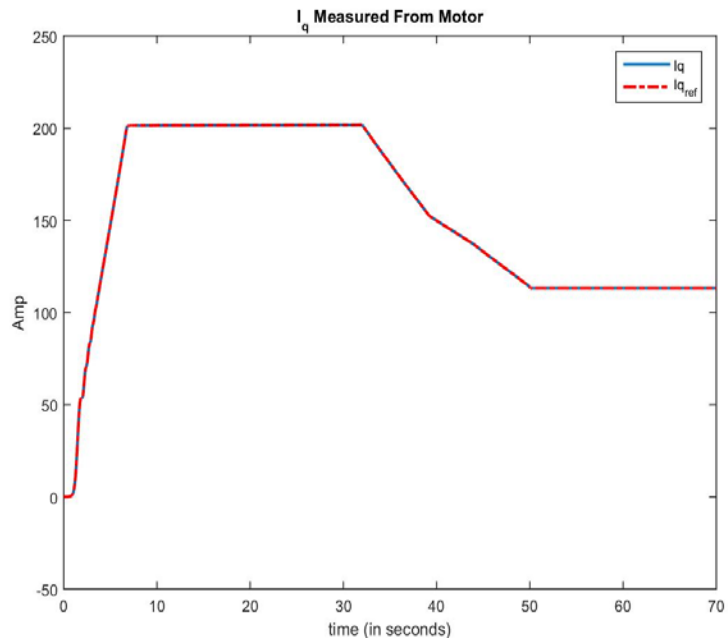

Figure 7.16: Test 3 ~ Q axis current (ref vs sim).

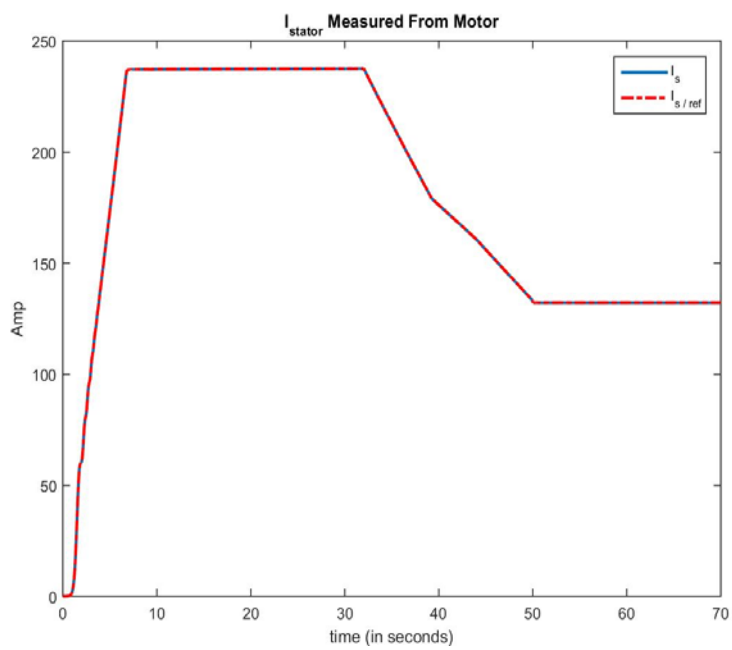

Figure 7.17: Test 3 ~ Stator current (ref vs sim).

From the simulation results presented here, the implemented control system shows reliable performances during the low speed constant torque region and during the high-speed constant power region. The error between the motor's final speed and the reference speed is small. Despite some torque ripples, the developed torque remains at a constant value at low speed with the MTPA control. While, the output power is roughly remaining at a constant value during FW region with the flux weakening control. From these simulation results, one can arrive at a conclusion that this flux weakening control algorithm is a valid flux-weakening control method.

8. COMMENTS

8.1 Conclusion

Current control of electric motor is important not only for torque control, but also for reaching maximum e_ciency. The various control methods have been simulated and compared to _nd their advantages and disadvantages. The DTC is often referred in literature as simple, which might be true for the math needed in the control systems calculations but during this project it has been quite tricky to get it to work properly. It has shown a high tendency to be very unstable, especially when considering the choice of the resistance parameter in the motor model and ux estimator. The DTC is also considered to have high torque and current ripple that can be somewhat reduced by decreasing the sample time, which has been proven to be correct. It would also be possible to reduce the ripple further by implementing some of the improvement of DTC suggested, such as Space Vector Modulation (SVM-DTC).

The FOC is normally considered to need more complex calculations to run, but with less torque and current ripple. The simulations have shown that the FOC has higher torque ripple then the DTC, but this is due to the choice to use hysteresis current control and not PI regulators. With the use of more precise current control and the use of SPWM or SVPWM it should be possible to reduce the torque ripple.

A robust control algorithm for PMSMs is proposed in this research that would achieve MPPA operation without needing phase current measurements. Most of the parameter dependent control schemes developed so far, do not include any technique to cope with unexpected changes in operating conditions. Conversely, schemes based on search algorithms appear to be robust against unexpected parameter variation, but suffer from poor dynamic response. The proposed method is rather a hybrid scheme, having a-priori knowledge as well as a search based algorithm.

The control mechanism is developed based on only the DC link power measurement, which makes the algorithm a cost effective solution. The self-converging nature of the algorithm makes it unsusceptible self-induced instability and reduces the risk of system failure. Stability analysis of the closed loop system also ensures a stable operating region of the scheme. The phase advance angle generation algorithm based on the estimation matrix ensures satisfactory dynamic performance when rapid variations in operating speed or load torque is introduced. Integration of the perturbation technique based on a gradient descent algorithm reduces the possibility of functioning in an inefficient region regardless of the operating condition and motor parameters. Further improvements were made by reducing switching loss using a minimum loss space vector PWM. Achieving MTPA trajectory without phase current feedback appeared to be a challenging task that was successfully performed by the control algorithm. Both simulation and experimental results validated the ability of the control scheme in attaining efficient operations.

8.2 Future Work

Although several developments were presented in this thesis, there are many interesting investigations left for the future work. Some possible subjects are listed as follows:

- The motor model used in the simulations included in this thesis can be replaced with a finite element motor model.
- Further investigations on motor's efficiencies at different operating points and by different control methods can be conducted. These significant investigations can be used to design optimal motors for full speed range operation and improve control methods for motors.
- Also it is important to reduce the torque ripples for the used control algoritms, in the light of inverter switching frequencies.
- The control parmeters were set according to the previously mentioned calculations, which utilized the single value for DQ axis inductances. İt will be helpful to update the PI control parameters according to the saturation levels in inductances, for getting solutions that are more realistic.

➢

REFERENCES

[1] **R. Saidur,** “A review on electrical motors energy use and energy savings,” *Renewable and Sustainable Energy Reviews*, vol. 14, no. 3, pp. 877–898, Apr. 2010.

[2] **B. C. Mecrow and a. G. Jack,** “Efficiency trends in electric machines and drives,” *Energy Policy*, vol. 36, no. 12, pp. 4336–4341, Dec. 2008.

[3] **A. Binder,** “Potentials for energy saving with modern drive technology — a survey,” in *Proc. of IEEE International Symposium on Power Electronics, Electrical Drives, Automation and Motion*, 2008, pp. 90–95.

[4] **C. T. Pan and S. M. Sue,** “A linear maximum torque per ampere control for IPMSM drives over full-speed range,” *IEEE Transactions on Energy Conversion*, vol. 20, no. 2, pp. 359–366, Jun. 2005.

[5] **Z. Zhu, Y. Chen, and D. Howe,** “Online optimal flux-weakening control of permanent-magnet brushless AC drives,” *IEEE Transactions on Industry Applications*, vol. 36, no. 6, pp. 1661–1668, 2000.

[6] **H. Murakami, Y. Honda, H. Kiriyama, S. Morimoto, and Y. Takeda,** “The performance comparison of SPMSM, IPMSM and SynRM in use as air-conditioning compressor,” in *Proc. of IEEE Industry Applications Society Annual Meeting*, 1999, vol. 2, pp. 840–845.

[7] **L. Chen, R. Davis, S. Stella, T. Tesch, and A. Fischer-Antze,** “Improved control techniques for IPM motor drives on vehicle application,” in *Proc. of IEEE Industry Applications Society Annual Meeting*, 2002, vol. 3, pp. 2051–2056.

[8] **B. H. Bae and S. K. Sul,** “Practical design criteria of interior permanent magnet synchronous motor for 42V integrated starter-generator,” in *Proc. of IEEE International Electric Machines and Drives Conference, (IEMDC)*, 2003, vol. 2, pp. 656–662.

[9] **D. Anton, K. Young-kwan, L. Sang-joon, and L. Sang-taek,** “Robust self-tuning MTPA algorithm for IPMSM drives,” in *Proc. of IEEE Industrial Electronics, (IECON)*, 2008, pp. 1355–1360.

[10] **P. Niazi, H. A. Toliyat, and A. Goodarzi,** “Robust maximum torque per ampere (MTPA) control of PM-assisted SynRM for traction applications,” *IEEE Transactions on Vehicular Technology*, vol. 56, no. 4, pp. 1538–1545, 2005.

[11] **P. C. Krause, O. Wasynczuk, S. D. Sudhoff, and S. Pekarek,** *Analysis of electric machinery and drive systems*. Wiley. com, 2013.

[12] **S. C. Carpiuc, D. I. Patrascu, and C. Lazar,** "Optimal torque control of the interior permanent magnet synchronous machine," in *Proc. of IEEE International Symposium on Information, Communication and Automation Technologies, (ICAT)*, 2011, pp. 1–8.

[13] **P. Pillay and R. Krishnan,** "Modeling, simulation, and analysis of permanent-magnet motor drives. II. The brushless DC motor drive," *IEEE Transactions on Industry Applications*, vol. 25, no. 2, pp. 274–279, 1989.

[14] **T. A. Lipo,** *Vector control and dynamics of AC drives*. Oxford University Press, USA, 1996.

[15] **K. Nakamura, K. Saito, and O. Ichinokura,** "Dynamic analysis of interior permanent magnet motor based on a magnetic circuit model," *IEEE Transactions on Magnetics*, vol. 39, no. 5, pp. 3250–3252, Sep. 2003.

[16] **Y. Yan, J. Zhu, H. Lu, Y. Guo, and S. Wang,** "Study of a PMSM model incorporating structural and saturation saliencies," in *Proc. of IEEE International Conference on Power Electronics and Drives Systems, (PEDS)*, 2007, pp. 575–580.

[17] **R. Nalepa and T. Orlowska-Kowalska,** "Optimum trajectory control of the current vector of a nonsalient-pole PMSM in the field-weakening region," *IEEE Transactions on Industrial Electronics*, vol. 59, no. 7, pp. 2867–2876, 2012.

[18] **R. Martis, N. Gupta, S. Sankar, and V. Rao**, "Permanent magnetic materials with low reversible temperature coefficient," *IEEE Transactions on Magnetics*, pp. 948–950, 1979.

[19] **T. Sebastian,** "Temperature effects on torque production and efficiency of PM motors using NdFeB magnets," *IEEE Transactions on Industry Applications*, vol. 3, no. 2, pp. 353–357, 1995.

[20] **Y. Zou,** M. Elbuluk, and Y. Sozer, "A complete modeling and simulation of induction generator wind power systems," in *Proc. of IEEE Industry Applications Society Annual Meeting*, 2010, no. 1, pp. 1–8.

[21] **R. H. Park,** "Two-reaction theory of synchronous machines generalized method of analysis-part I," *Transactions of the American Institute of Electrical Engineers*, vol. 48, no. 3, pp. 716–727, Jul. 1929.

[22] **P. Pillay and R. Krishnan,** "Modeling, simulation, and analysis of permanent-magnet motor drives. I. The permanent-magnet synchronous motor drive," *IEEE Transactions on Industry Applications*, vol. 25, no. 2, pp. 265–273, 1989.

[23] **P. Pillay and R. Krishnan,** "Modeling of permanent magnet motor drives," in *Proc. of Robotics and IECON Conferences*, 1987, pp. 289–293.

[24] **A. Consoli, G. Scarcella, G. Scelba, and A. Testa,** "Steady-state and transient operation of IPMSMs under maximum-torque-per-ampere control," *IEEE Transactions on Industry Applications*, vol. 46, no. 1, pp. 121–129, 2010.

[25] **A. Consoli, G. Scarcella, G. Scelba, and S. Sindoni, "**Modeling control of IPM synchronous motors," in *Proc. of IEEE Power and Energy Society General Meeting-Conversion and Delivery of Electrical Energy in the 21st Century*, 2008, pp. 1–6.

[26] **J. Kang,** "General purpose permanent magnet motor drive without speed and position sensor," *Yaskawa Electric Corp., Japan, Yaskawa Application Note WP. AFD*.

[27] **T. M. Jahns, G. B. Kliman, and T. W. Neumann,** "Interior permanent-magnet synchronous motors for adjustable-speed drives," *IEEE Transactions on Industry Applications*, vol. IA-22, no. 4, pp. 738–747, Jul. 1986.

[28] **S.Y. Jung, J. Hong, and K. Nam,** "Current minimizing torque control of IPMSM using Ferrari's method," *IEEE Transactions on Power Electronics*, vol. 28, no. 12, pp. 5603–5617, 2013.

[29] **G. Cardano,** *The Rules of Algebra (Ars Magna), translated and edited by T. Richard Witmer*. Dover Publications, Inc., Mineola, 2007.

[30] **H. Kim, J. Hartwig, and R. D. Lorenz,** "Using on-line parameter estimation to improve efficiency of IPM machine drives," in *Proc. of IEEE Power Electronics Specialists Conference, (PESC)*, 2002, vol. 2, pp. 815–820.

[31] **Y.S. Kim and S.K. Sul,** "Torque control strategy of an IPMSM considering the flux variation of the permanent magnet," in *Proc. of IEEE Industry Applications Society Annual Meeting*, 2007, pp. 1301–1307.

[32] **S. Morimoto, M. Sanada, and Y. Takeda,** "Wide-speed operation of interior permanent magnet synchronous motors with high-performance current regulator," *IEEE Transactions on Industry Applications*, vol. 30, no. 4, pp. 920–926, 1994.

[33] **S. Morimoto, T. Ueno, M. Sanada, A. Yamagiwa, Y. Takeda, and T. Hirasa**, "Effects and compensation of magnetic saturation in permanent magnet synchronous motor drives," in *Proc. of IEEE Industry Applications Society Annual Meeting*, 1993, no. 2, pp. 59–64.

[34] **R. Bellman,** "Dynamic programming and Lagrange multipliers," in *Proc. of the National Academy of Sciences of the United States of America*, 1956, vol. 42, p. 767.

[35] **S. Morimoto, K. Hatanaka, Y. Tong, Y. Takeda, and T. Hirasa,** "Servo drive system and control characteristics of salient pole permanent magnet synchronous motor," *IEEE Transactions on Industry Applications*, vol. 29, no. 2, pp. 338–343, 1993.

[36] **Y. R. Mohamed and T. K. Lee,** "Adaptive self-tuning MTPA vector controller for IPMSM drive system," *IEEE Transactions on Energy Conversion*, vol. 21, no. 3, pp. 636–644, Sep. 2006.

[37] **G. C. Goodwin and K. S. Sin,** *Adaptive filtering prediction and control*. Courier Dover Publications, 2013.

[38] **G. Rang, J. Lim, K. Nam, H. Bin Ihm, and H. G. Kim,** "A MTPA control scheme for an IPM synchronous motor considering magnet flux variation caused by temperature," in *Proc. of IEEE Applied Power Electronics Conference and Exposition (APEC)*, 2004, vol. 3, no. 5, pp. 1617–1621.

[39] **C. Mademlis, I. Kioskeridis, and N. Margaris,** "Optimal efficiency control strategy for interior permanent-magnet synchronous motor drives," *IEEE Transactions on Energy Conversion*, vol. 19, no. 4, pp. 715–723, Dec. 2004.

[40] **R. S. Colby and D. W. Novotny,** "An efficiency-optimizing permanent-magnet," *IEEE Transactions on Industry Applications*, vol. 24, no. 3, pp. 462–469, 1988.

[41] **S. Kim, Y.D. Yoon, S.K. Sul, K. Ide, and K. Tomita,** "Parameter independent maximum torque per ampere (MTPA) control of IPM machine based on signal injection," in *Proc. of IEEE Applied Power Electronics Conference and Exposition (APEC)*, 2010, no. 1, pp. 103–108.

[42] **S. Bolognani, R. Petrella, A. Prearo, and L. Sgarbossa,** "Automatic tracking of MTPA trajectory in IPM motor drives based on AC current injection," *IEEE Transactions on Industry Applications*, vol. 47, no. 1, pp. 105–114, Jan. 2011.

[43] **A. Consoli and A. Abela,** "Transient performance of permanent magnet AC motor drives," *IEEE Transactions on Industry Applications*, vol. IA-22, no. 1, pp. 32–41, Jan. 1986.

[44] **D. W. Marquardt,** "An algorithm for least-squares estimation of nonlinear parameters," *Journal of the Society for Industrial & Applied Mathematics*, vol. 11, pp. 431–441, 1963.

[45] **M. Haque and M. Rahman,** "Dynamic model and parameter measurement of interior permanent magnet synchronous motor," in *Proc. of Australasian Universities Power Engineering Conference (AUPEC)*, 2006, pp. 10–13.

[46] **Y. Sozer and D. A. Torrey,** "Adaptive torque ripple control of permanent magnet brushless DC motors," in *Proc. of IEEE Applied Power Electronics Conference and Exposition (APEC)*, 1998, pp. 86–92.

[47] **Y. Sozer, H. Kaufman, and D. A. Torrey,** "Direct model reference adaptive control of permanent magnet brushless DC motors," in *Proc. of the 1997 IEEE International Conference on Control Applications*, 1997, pp. 633–638.

[48] **Z. Gajic,** *Linear dynamic systems and signals*. Prentice Hall/Pearson Education, 2003.

[49] **G. B. Arfken, H. J. Weber, and L. Ruby,** *Mathematical methods for physicists*. Academic press, 2005.

[50] **R. Kazmierkowski, Marian P and Krishnan,** *Control in power electronics: selected problems*. Academic press, 2002.

[51] **V. Der Broeck, H. Willi, H. C. Skudelny, and G. V. Stanke,** "Analysis and realization of a pulsewidth modulator based on voltage space vectors," *IEEE Transactions on Industry Applications*, vol. 24, no. 8716204, pp. 142–150, 1988.

[52] **A. M. Trzynadlowski and S. Legowski,** "Minimum-loss vector PWM strategy for three-phase inverters," *IEEE Transactions on Power Electronics*, vol. 9, no. 1, pp. 26–34, 1994.

[53] **Y. Sozer,** "Direct adaptive control of permanent magnet motors," Rensselaer Polytechnic Institute, 2000.

[54] **Y. Zou,** "Modeling, control and maximum power point tracking (MPPT) of doubly-fed induction generator (DFIG) wind power system," University of Akron, 2012.

CURRICULUM VITAE

Name Surname: Ahmet Halit ÜNSAL

Place and Date of Birth: Turkey 08.03.1989

E-Mail: aunsal89@gmail.com

EDUCATION: Iowa State University

B.Sc.: Electrical and Electronics Engineering